A multiaxial constitutive model for concrete in the fire situation: Theoretical formulation.

Thomas Gernay[a], Alain Millard[b] and Jean-Marc Franssen[c]

[a] The National Fund for Scientific Research, Structural Engineering Department, University of Liege, Ch. Des Chevreuils 1, 4000 Liege, Belgium, T.Gernay@alumni.ulg.ac.be, tel. +32(0)43669245, fax. +32(0)43669534.

[b] CEA, DEN, DANS, DM2S, SEMT, LM2S, F-91191 Gif sur Yvette, France, Alain.Millard@cea.fr

[c] Structural Engineering Department, University of Liege, Ch. Des Chevreuils 1, 4000 Liege, Belgium, JM.Franssen@ulg.ac.be

ABSTRACT

This paper aims to develop a multiaxial concrete model for implementation in finite element softwares dedicated to the analysis of structures in fire. The need for proper concrete model remains a challenging task in structural fire engineering because of the complexity of the concrete mechanical behavior characterization and the severe requirements for the material models raised by the development of performance-based design. A fully three-dimensional model is developed based on the combination of elastoplasticity and damage theories. The state of damage in concrete, assumed isotropic, is modeled by means of a fourth order damage tensor to capture the unilateral effect. The concrete model comprises a limited number of parameters that can be identified by three simple tests at ambient temperature. At high temperatures, a generic transient creep model is included to take into account explicitly the effect of transient creep strain. The numerical implementation of the concrete model in a finite element software is presented and a series of numerical simulations are conducted for validation. The concrete behavior is accurately captured in a large range of temperature and stress states. A limitation appears when modeling the concrete post-peak behavior in highly confined stress states, due to the coupling assumption between damage and plasticity, but the considered levels of triaxial confinement are unusual stress states in structural concrete.

Keywords: thermomechanical processes; concrete; constitutive behavior; elastic-plastic material; damage model; fire.

Highlights:

- A plastic-damage model for concrete at high temperature is proposed.
- The unilateral effect is captured by a fourth-order damage tensor.
- Transient creep strain is explicitly included in the model.
- The model captures the main thermomechanical phenomena exhibited by concrete.
- The implications of the coupling between plasticity and damage are discussed.

1 Introduction

1.1. Modeling the concrete mechanical behavior in structural fire engineering

Although structural concrete is widely used in civil engineering, proper modelling of its thermo-mechanical behavior remains a challenging issue for engineers because of the complexity of the phenomena that result from the microcracking process in this material. Concrete is a complex composite material composed by aggregates and hydrated cement paste. The concrete mechanical behavior is highly nonlinear and influenced by microcracking, which causes softening behavior, stiffness degradation and unilateral effect. In compression, concrete exhibits inelastic volumetric expansion referred to as dilatancy in the literature; this phenomenon has a significant effect on the behavior of plain and reinforced concrete structures in multiaxial stress states (Lee and Fenves, 1998). In addition, the behavior is affected by other characteristic phenomena at elevated temperatures such as explosive spalling or transient creep.

The difficulty to develop a concrete model suitable for the analysis of structures at high temperatures is also due to the severe requirements for the material models raised by the development of performance-based design. The increased use of performance-based approach for fire safety is related to the search for achieving fire safety through alternative, cost effective solutions (Meacham and Custer, 1992; Kodur, 1999). Performance-based design has extended the frontiers of the analysis, studying the response of entire structures instead of isolated structural elements or assuming natural fire scenarios instead of standard fires such as the ASTME fire (ASTME, 2007) or the ISO fire (ISO, 1975). As a consequence, the material models must be sufficiently robust for complex numerical calculations such as, for instance, the analysis of tensile membrane action in composite slabs. Besides, the models must be valid also during the cooling down phase of a natural fire and therefore the evolution of the material properties with decreasing temperatures must be established. Finally, the will to make available the models for practical applications in real projects leads to the necessity to limit the number of parameters in the models and to ensure an easy identification of these parameters by elementary tests.

1.2. Review of the concrete models

Plasticity theory offers a very interesting framework for modelling concrete because this theory is nowadays theoretically consolidated and computationally efficient (Wu, et al., 2006) and it is suitable for capturing the phenomena of dilatancy, permanent strain and hardening and softening behavior of the material (Feenstra and de Borst, 1996; Lee and Fenves, 1998). The split of strains into elastic and plastic parts within the plasticity theory allows for convenient modelling of the inelastic deformations in concrete. Many researchers have used plasticity theory alone to model the concrete behavior (William and Warnke, 1974; Onate, et al., 1993; Feenstra and de Borst, 1996; Grassl, et al., 2002; Li and Crouch, 2010). The published models frequently use non-associative flow rules in order to capture the dilatancy in compression, and work or strain hardening to model the hardening and softening of the material. However, plasticity models are unable to address the process of damage due to microcracks growth, and therefore they fail to reproduce some of the phenomena observed

in experiments such as the stiffness degradation and unilateral effect (Wu, et al., 2006). The unilateral effect is the sudden recovery of material stiffness during unloading from the tensile region to the compressive region, due to closure of the tensile cracks. As a consequence, recent research on concrete modelling tends to develop models that combine plasticity theory with other theories more suitable for the description of the concrete behavior in tension, such as fracture theory (Cervenka and Papanikolaou, 2008) or damage theory.

Continuum damage mechanics (CDM) is commonly used for modelling concrete behavior; damage models rely on the assumption that the degradation due to micro-cracking can be taken into account through the variations of the elastic properties. Therefore damage models are particularly suitable for description of stiffness degradation and unilateral effect in concrete. Extensive research work has been performed on concrete modelling in the framework of CDM, in which damage is considered as an isotropic (e.g. Mazars, 1984; Lee and Fenves, 1998; Grassl and Jirasek, 2006; Wu, et al., 2006; Richard, et al., 2010) or an anisotropic process (e.g. Ortiz, 1985; Carol, et al., 2001a-b; Desmorat, et al., 2007; Voyiadjis, et al., 2008; Abu Al-Rub and Voyiadjis, 2009). Although CDM provides many advantages for modelling concrete, it is not suitable for capturing some important observed phenomena such as irreversible deformations and inelastic volumetric expansion (dilatancy) in compression. Therefore the combination of CDM with plasticity theory is certainly appealing to encompass the advantages of the two approaches in a single constitutive model and this approach has been elected in the present work.

Constitutive models for concrete at ambient temperature based on plastic-damage formulation have been proposed by several authors. These models usually combine stress-based plasticity with either isotropic or anisotropic damage. Models coupling plasticity with anisotropic damage address the characterization of the concrete damage behavior with different microcracking in different directions (Meschke, et al., 1998; Cicekli, et al., 2007; Voyiadjis, et al., 2008; Voyiadjis, et al., 2009). However, modeling anisotropic damage in concrete is complex; see for instance the works of Carol et al. (2001a-b). It has been noted by several authors that the applicability to structural analysis of anisotropic damage models for concrete is not straightforward due to the inherent complexities of the required numerical algorithms (Grassl and Jirasek, 2006; Wu, et al., 2006). As a consequence, isotropic damage has been widely used for concrete in combination with plasticity (Lee and Fenves, 1998; Krätzig and Pölling, 2004; Grassl and Jirasek, 2006; Taqieddin, et al., 2012). The isotropic damage process can be characterized by one scalar, several scalars or a tensor. Yet, the one-scalar damage models are not adapted for concrete even when damage is modeled as an isotropic process. The use of different scalars to capture the damage process in concrete (Mazars, 1984; Lee and Fenves, 1998) is consistent with the experimental observation of different damage mechanisms developing in tension and in compression; a minimum of two scalar variables is necessary to describe these different damage mechanisms. Some authors have proposed a fourth-order damage tensor to characterize the state of isotropic damage in concrete (Ju, 1990; Wu, et al., 2006), showing that a fourth-order tensor is required to capture the unilateral effect; in fact, even for isotropic damage, proper description of the damage state in concrete requires a fourth-order tensor based on two scalar variables.

Among the published plastic-damage models, stress-based plasticity is formulated either in the effective stress space (Lee and Fenves, 1998; Grassl and Jirasek, 2006; Wu, et al.,

2006; Cicekli, et al., 2007; Saritas and Filippou, 2009) or in the nominal (damaged) stress space (Lubliner, et al., 1989; Krätzig and Pölling, 2004; Voyiadjis, et al., 2008; Taqieddin, et al., 2012). According to the generally adopted nomenclature, effective stress $\bar{\sigma}$ is meant as the average micro-level stress applied to the undamaged volume of the material whereas nominal stress σ is meant as the macro-level stress and is defined as force divided by the total area. Formulation of the plastic response in the effective stress space relies on the assumption that plastic flow occurs in the undamaged material micro-bounds by means of effective quantities (Ju, 1989). It has been shown that local uniqueness is always guaranteed for the plastic-damage models with plasticity formulated in the effective stress space, whereas local uniqueness requires severe restriction when plasticity is formulated in the nominal stress space (Grassl and Jirasek, 2006). Besides, other authors have noted that plastic-damage models formulated in the effective stress space are numerically more stable and attractive compared with models formulated in the nominal stress space (Abu Al-Rub and Voyiadjis, 2009). Formulation of the plastic response in the effective stress space allows for decoupling the plastic part from the damage part in the computation process; computation of the plastic response then constitutes a standard elastoplastic problem in the effective stress space. As a result, the combination of stress-based plasticity formulated in the effective stress space and isotropic damage constitutes an interesting approach for modelling the behavior of concrete.

Elevated temperatures are the cause of degradations at the micro-level that result in loss of stiffness and strength of the material. Elevated temperatures in concrete may also cause specific phenomena such as transient creep or explosive spalling, which have an influence on the structural response. Concrete models taking into account the effect of high temperatures and based on the plasticity theory have been developed by Khennane and Baker (1992) and Heinfling (1998); this latter contribution notably takes into account the increasing temperature sensitivity of compressive strength to hydrostatic pressure. Other authors have developed concrete models at high temperatures based on the damage theory (Gawin, et al., 2004; Baker and de Borst, 2005). These damage models use a thermal damage variable to capture the degradation of elastic modulus with temperature. Although the theoretical framework of plastic-damage formulation has been found appealing by many researchers for modeling concrete at ambient temperature, the development of concrete plastic-damage models at high temperature has been hardly treated in the literature. Nechnech et al. (2002) proposed an interesting contribution which highlighted the interest of plastic-damage models for concrete at high temperature. This latter model also uses a thermal damage to account for the temperature variation of the elastic modulus and it incorporates the effect of transient creep using Anderberg and Thelandersson's formula (1976). However, the modeling of damage by two scalars did not allow for capturing the unilateral effect and the authors had to introduce a specific parameter in the model to get around this limitation. Besides, the model was only developed in plane stress states and its applicability for practical applications of structural fire engineering has not been demonstrated beyond the analysis of one-way reinforced concrete slabs supported on two sides and subjected to heating. Consequently, research efforts are still required to give further insight into concrete modelling at elevated temperature and to extend the latest developments of ambient temperature models to elevated temperature, with special emphasis on the specific demands raised by the development of performance-based design.

1.3. Significance of the research work

This paper proposes a new multiaxial constitutive model for concrete in the fire situation based on the theoretical background of elastoplasticity and damage theories. The model extends to high temperatures several developments recently published for concrete modeling at ambient temperature and it incorporates original contributions notably for the evolution laws and for the transient creep strain. Following the requirements raised by performance-based design, special care is given to the numerical robustness of the model and the influence of the stress-temperature history on the strain response of the material. A series of numerical simulations of building structures in fire will be presented in a forthcoming paper for validating the applicability of the concrete model to structural fire engineering applications.

2 Plastic-damage model for concrete

2.1. Constitutive relationships

The mechanical behavior of concrete at elevated temperatures is captured by constitutive relationships between the total strain tensor and the stress tensor. Assuming small strains, the total strain $\underline{\underline{\varepsilon}}_{tot}$ is decomposed into elastic strain $\underline{\underline{\varepsilon}}_{el}$, plastic strain $\underline{\underline{\varepsilon}}_{p}$, free thermal strain $\underline{\underline{\varepsilon}}_{th}$ and transient creep strain $\underline{\underline{\varepsilon}}_{tr}$ according to Eq. (1).

$$\underline{\underline{\varepsilon}}_{tot} = \underline{\underline{\varepsilon}}_{el} + \underline{\underline{\varepsilon}}_{p} + \underline{\underline{\varepsilon}}_{th} + \underline{\underline{\varepsilon}}_{tr} \tag{1}$$

The sum of the elastic strain and the plastic strain is referred to as instantaneous stress-related strain $\underline{\underline{\varepsilon}}_{\sigma}$.

Basic creep, defined as the additional strain that develops when only time is changing with all other conditions such as stress and temperature being constant, is generally omitted for the structural calculation of building structures in the fire situation because, in this situation, this strain is often very small compared to the other strains in concrete due to the short period of the fire (Li and Purkiss, 2005). If necessary, it could easily be added to the strain decomposition in Eq. (1).

The characterization of plastic response is formulated in the effective stress space. The strain equivalence hypothesis is adopted here, which means that the strain in the effective (undamaged) and nominal (damaged) configurations are equal. Considering that the plastic behavior occurs in the undamaged material, the constitutive relationship in the effective stress space can be written following the classical elastoplastic behavior. The elastic strain tensor is thus related to the effective stress tensor $\underline{\underline{\bar{\sigma}}}$ by means of the fourth-order isotropic linear-elastic stiffness tensor $\underline{\underline{\underline{\underline{C}}}}_{0}$, see Eq. (2). The plastic response accounts for the development of irreversible strains in the material.

$$\underline{\underline{\bar{\sigma}}} = \underline{\underline{\underline{\underline{C}}}}_{0} : \underline{\underline{\varepsilon}}_{el} = \underline{\underline{\underline{\underline{C}}}}_{0} : \left(\underline{\underline{\varepsilon}}_{tot} - \underline{\underline{\varepsilon}}_{th} - \underline{\underline{\varepsilon}}_{tr} - \underline{\underline{\varepsilon}}_{p} \right) = \underline{\underline{\underline{\underline{C}}}}_{0} : \left(\underline{\underline{\varepsilon}}_{\sigma} - \underline{\underline{\varepsilon}}_{p} \right) \tag{2}$$

To capture the effects of microcracking on the elastic properties of the material, damage is introduced in the model using a fourth-order isotropic damage tensor $\underline{\underline{\underline{\underline{D}}}}$. This fourth-order damage tensor is used to map the effective stress tensor $\underline{\underline{\bar{\sigma}}}$ into the nominal stress tensor $\underline{\underline{\sigma}}$ according to Eq. (3), where $\underline{\underline{\underline{\underline{I}}}}$ is the fourth-order identity tensor.

$$\underline{\underline{\sigma}} = \left(\underline{\underline{\underline{\underline{I}}}} - \underline{\underline{\underline{\underline{D}}}}\right) : \underline{\underline{\bar{\sigma}}} \tag{3}$$

As the damage mechanisms that develop in concrete are different in tension and in compression, a damage scalar internal variable d_t is considered for modelling of tensile damage and a damage scalar internal variable d_c is considered for modeling of compressive damage. The damage tensor is calculated from these two damage scalars using Eq. (4), which has been proposed by Wu, et al. (2006).

$$\underline{\underline{\underline{\underline{D}}}} = d_t \, \underline{\underline{\underline{\underline{P}}}}^{+} + d_c \, \underline{\underline{\underline{\underline{P}}}}^{-} \tag{4}$$

In this latter equation, $\underline{\underline{\underline{\underline{P}}}}^{+}$ and $\underline{\underline{\underline{\underline{P}}}}^{-}$ are the fourth-order projection tensors calculated according to Eq. (5)

$$\underline{\underline{\underline{\underline{P}}}}^{+} = \sum_i H\left(\bar{\sigma}_i\right)\left(\underline{\underline{p}}_{ii} \otimes \underline{\underline{p}}_{ii}\right), \quad \underline{\underline{\underline{\underline{P}}}}^{-} = \underline{\underline{\underline{\underline{I}}}} - \underline{\underline{\underline{\underline{P}}}}^{+} \tag{5}$$

where $H\left(\bar{\sigma}_i\right)$ is the Heaviside function computed for the *i*th eigenvalue $\bar{\sigma}_i$ of $\underline{\underline{\bar{\sigma}}}$, and the second-order tensor $\underline{\underline{p}}_{ii}$ is defined by Eq. (6), with $\underline{n}_i$ the *i*th normalized eigenvector corresponding to $\bar{\sigma}_i$.

$$\underline{\underline{p}}_{ij} = \underline{\underline{p}}_{ji} = \frac{1}{2}\left(\underline{n}_i \otimes \underline{n}_j + \underline{n}_j \otimes \underline{n}_i\right) \tag{6}$$

The fourth-order projection tensors are built to allow for a decomposition of the effective stress tensor $\underline{\underline{\bar{\sigma}}}$ into positive and negative components according to Eq. (7).

$$\underline{\underline{\bar{\sigma}}}^{+} = \underline{\underline{\underline{\underline{P}}}}^{+} : \underline{\underline{\bar{\sigma}}} \ , \qquad \underline{\underline{\bar{\sigma}}}^{-} = \underline{\underline{\bar{\sigma}}} - \underline{\underline{\bar{\sigma}}}^{+} = \underline{\underline{\underline{\underline{P}}}}^{-} : \underline{\underline{\bar{\sigma}}} \tag{7}$$

Consequently, the tensile damage scalar d_t only affects the positive part of the effective stress tensor whereas the compressive damage scalar d_c only affects the negative part of the effective stress tensor: $\underline{\underline{\sigma}} = \left(1 - d_t\right)\underline{\underline{\bar{\sigma}}}^{+} + \left(1 - d_c\right)\underline{\underline{\bar{\sigma}}}^{-}$. When the stress state in the material changes from tension to compression, the effect of the tensile damage scalar d_t on the macroscopic behavior disappear, which corresponds physically to the closure of the tensile cracks and subsequent stiffness recovery in concrete. Thus, this representation of the state of damage allows for capturing properly the unilateral effect, as can be seen in Fig. 1; in this figure, the model response to a unilateral test is compared with experimental data given by Ramtani (1990).

2.2. Plastic theory

A multi-surface yield criterion is adopted to capture the behavior of concrete under different load paths. The use of dedicated yield surfaces for tension and for compression is convenient in concrete as this material exhibits a non-symmetrical behavior driven by different failure modes in tension and in compression. Feenstra and de Borst (1996) have proposed a multi-surface model for concrete in biaxial stress states combining the Drucker-Prager criterion with the Rankine cutoff in tension. The same approach is adopted here for the concrete model in three-dimensional stress states, leading to the expressions of Eq. (8a) and Eq. (8b). In these equations, F_t is the Rankine yield function, $\bar{\sigma}_I$ is the maximum principal effective stress, $\bar{\tau}_t$ is the tensile hardening function depending on the tensile hardening parameter κ_t, F_c is the Drucker-Prager yield function, $\bar{I}_1$ is the trace (first invariant) of the effective stress tensor, $\bar{J}_2$ is the second invariant of the deviatoric effective stress tensor, $\bar{\tau}_c$ is the compressive hardening function depending on the compressive hardening parameter κ_c and α is a material parameter (coefficient of internal friction) defined by $\alpha = (f_b - f_c)/(2f_b - f_c)$, where f_c and f_b respectively represent the uniaxial and biaxial compressive strength of the material. The expressions of Eq. (8a-b) are written in terms of effective stress as the plastic response applies to the undamaged part of the material.

$$\begin{cases} F_t\left(\bar{\underline{\underline{\sigma}}}, \kappa_t\right) = \bar{\sigma}_I - \bar{\tau}_t\left(\kappa_t\right) \le 0 & \text{(8a)} \\ F_c\left(\bar{\underline{\underline{\sigma}}}, \kappa_c\right) = \sqrt{3\bar{J}_2} + \alpha\,\bar{I}_1 - (1-\alpha)\,\bar{\tau}_c\left(\kappa_c\right) \le 0 & \text{(8b)} \end{cases}$$

The multi-surface yield criterion that results from the combination of Rankine yield function and Drucker-Prager yield function is plotted in the two-dimensional stress space, i.e. assuming that $\sigma_{III} = 0$, in Fig. 2. The limit yield function corresponds to the failure envelope at the end of the hardening process; this limit yield function agrees with experimental data of the biaxial failure envelope given by Kupfer and Gerstle (1973). It is assumed that the yield function experiences isotropic hardening/softening; the value of the yield function at a certain stage of this hardening/softening process is also plotted in Fig. 2.

Plastic flow rules have to be postulated to govern the evolution of plastic flow when the effective stress state reaches the yield surfaces. As concrete is a frictional material, in which dilatancy occurs when loaded in compression, a non-associated flow rule is adopted in compression. The plastic potential G_c is given by $G_c = \sqrt{3\bar{J}_2} + \alpha_g\,\bar{I}_1$, where α_g is a dilatancy parameter. The physical interpretation of this expression is that the compressive flow is associated in the deviatoric plane but its volumetric part uses a dilatancy coefficient α_g different from the coefficient of internal friction α (Feenstra and de Borst, 1996). In tension, an associated flow rule is used and the plastic potential G_t is thus taken equal to the plastic yield function: $G_t = F_t$.

According to Koiter's rule (1953), the total plastic strain rate tensor can be obtained as the sum of the tensile and the compressive plastic strain rate tensors, according to Eq. (9).

$$\dot{\underline{\underline{\varepsilon}}}_p = \dot{\underline{\underline{\varepsilon}}}_p^t + \dot{\underline{\underline{\varepsilon}}}_p^c = \dot{\lambda}_t \frac{\partial F_t}{\partial \underline{\underline{\bar{\sigma}}}} + \dot{\lambda}_c \frac{\partial G_c}{\partial \underline{\underline{\bar{\sigma}}}} \tag{9}$$

The plastic multipliers $\dot{\lambda}_t$ and $\dot{\lambda}_c$ can be determined using the Kuhn-Tucker conditions and the consistency requirements respectively expressed by Eq. (10) and Eq. (11).

$$\dot{\lambda}_j \geq 0\,, \quad F_j\left(\underline{\underline{\bar{\sigma}}}, \kappa_j\right) \leq 0\,, \quad \dot{\lambda}_j\, F_j\left(\underline{\underline{\bar{\sigma}}}, \kappa_j\right) = 0 \quad \big| \quad j = t, c \tag{10}$$

$$\dot{\lambda}_j\, \dot{F}_j\left(\underline{\underline{\bar{\sigma}}}, \kappa_j\right) = 0 \quad \big| \quad j = t, c \tag{11}$$

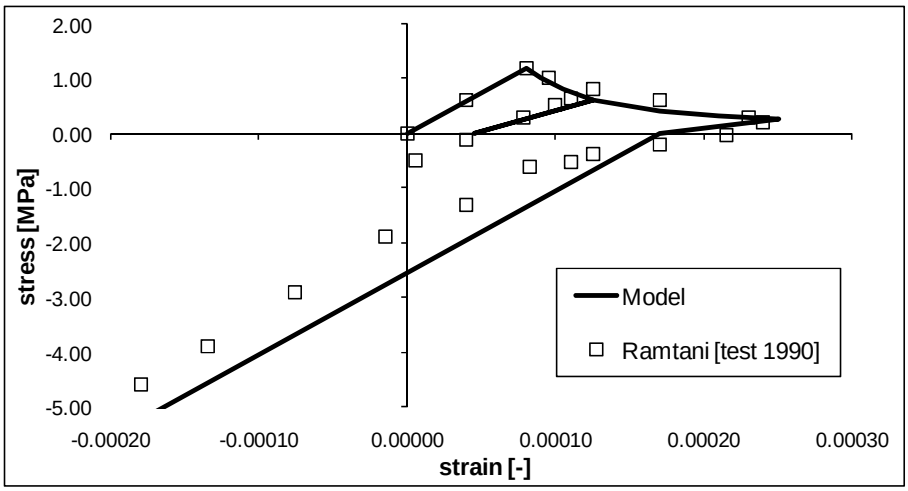

Fig. 1: The use of a fourth-order damage tensor allows for modeling the unilateral effect in concrete.

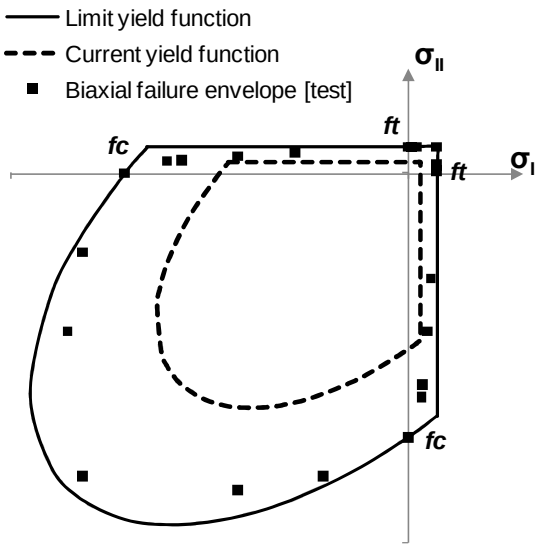

Fig. 2: Multi-surface yield criterion plotted in the two-dimensional principal stress space

The hardening variables κ_t and κ_c respectively govern the evolution of the Rankine and the Drucker-Prager yield surfaces; this evolution is made by isotropic hardening/softening. In fact, the hardening variables are the plastic internal variables that characterize the plastic state of the material; they can be considered as indicators of the degree of yielding in the material and therefore are called accumulated plastic strains. These hardening variables are induced by plastic flow and they can be related to the plastic multipliers. Adopting a work-hardening hypothesis and assuming that the yielding mechanisms in tension and in compression are decoupled, the evolution of the hardening variables is given by: $\dot{\kappa}_t = \dot{\lambda}_t \geq 0$ and $\dot{\kappa}_c = \dot{\lambda}_c \geq 0$.

The hardening variables can then be interpreted as effective plastic strain, although the formula in compression is adapted for non associated flow, see Eq. (12a) and Eq. (12b).

$$\dot{\kappa}_t = \left(\overline{\underline{\underline{\sigma}}} : \dot{\underline{\underline{\varepsilon}}}_p^t\right) \Big/ \overline{\tau}_t \tag{12a}$$

$$\dot{\kappa}_c = \left(\overline{\underline{\underline{\sigma}}} : \dot{\underline{\underline{\varepsilon}}}_p^c\right) \Big/ G_c \tag{12b}$$

The rate equations of the hardening variables can be expressed in the uniaxial case to give a more direct interpretation of these variables. Under uniaxial tension in direction *x*, the Rankine yield function leads to the equality $\overline{\sigma}_x = \overline{\tau}_t\left(\kappa_t\right)$ during the yielding process and Eq. (12a) turns into $\dot{\kappa}_t = \dot{\varepsilon}_{p,x}^t$, so that it is possible to identify the tensile hardening law from the stress-strain curve in uniaxial tension. Similar developments in uniaxial compression lead to $\left|\overline{\sigma}_x\right| = \overline{\tau}_c\left(\kappa_c\right)$ during the yielding process, with $\overline{\sigma}_x < 0$ the effective stress, and $\dot{\kappa}_c = \dot{\varepsilon}_{p,x}^c \Big/ \left(\alpha_g - 1\right)$. The compressive hardening parameter is proportional to the plastic strain in the direction of applied stress and it is possible to identify the compressive hardening law from the stress-strain curve in uniaxial compression.

The hardening functions $\overline{\tau}_t$ and $\overline{\tau}_c$ have the meaning of current uniaxial tensile and compressive strength of the material. However, these functions are written in the effective stress space and therefore they cannot be determined by direct identification with the experimental uniaxial stress-strain curves, which are in the nominal (apparent) stress space. The relationships between the effective and the nominal hardening functions are given by $\tau_t\left(\kappa_t\right) = \left(1 - d_t\right)\overline{\tau}_t\left(\kappa_t\right)$ and $\tau_c\left(\kappa_c\right) = \left(1 - d_c\right)\overline{\tau}_c\left(\kappa_c\right)$, respectively. In these equations, τ_t and τ_c are the tensile and compressive hardening functions in the nominal stress space; therefore these functions can be directly identified to the current uniaxial tensile and compressive strengths of the material. The functions $\overline{\tau}_t$ and $\overline{\tau}_c$ can then be derived once the damage scalars d_t and d_c have been defined.

In uniaxial tension, the response in nominal (i.e. apparent) stress is elastic until peak stress, followed by a material softening until failure. The experimentally observed decrease of the uniaxial tensile strength with the strain can be modeled by a curve tending to zero-stress level asymptotically (Fig. 3). Consequently, the softening function is described by a combination of negative exponentials according to Eq. (13). The expression of Eq. (13) results from a numerical calibration on experimental data. In this equation, a_t is a non

dimensional model parameter to be determined and f_t is the uniaxial tensile strength (i.e. peak stress).

$$\tau_t(\kappa_t) = \left[\frac{1}{2}\exp(-a_t\ \kappa_t) + \frac{1}{2}\exp(-6\ a_t\ \kappa_t)\right] f_t \tag{13}$$

In uniaxial compression, the concrete behavior presents first an elastic domain until the compressive limit of elasticity f_{c0}, followed by a hardening branch until the stress reaches the compressive strength f_c and finally a softening branch until failure. This behavior is modeled by the relationships of Eq. (14) in the nominal stress space. In this equation, κ_{c1} is the accumulated plastic strain in compression at peak stress such that $\tau_c(\kappa_{c1}) = f_c$, and b_c is a model parameter to be determined. The first expression of Eq. (14), which represents the hardening branch, is written following a similar formulation as the expression prescribed in the Eurocode 2 part 1-2 (2004-a). This formulation was adopted to ensure the consistency of the present multiaxial concrete model with the uniaxial concrete model of Eurocode, which is widely used in practical applications. Application of the multiaxial model therefore yields similar results as the Eurocode formula in a situation of uniaxial compression. The hardening laws in tension and compression are plotted in the nominal stress space in Fig. 3.

$$\begin{cases} \tau_c(\kappa_c) = f_{c0} + \dfrac{2(f_c - f_{c0})\,\kappa_c}{\kappa_{c1}\left(1 + \left(\dfrac{\kappa_c}{\kappa_{c1}}\right)^2\right)} & \text{if } \kappa_c \le \kappa_{c1} \\ \tau_c(\kappa_c) = f_c\left(1 + b_c(\kappa_c - \kappa_{c1})\right)\exp\left(-b_c(\kappa_c - \kappa_{c1})\right) & \text{if } \kappa_c \ge \kappa_{c1} \end{cases} \tag{14}$$

2.3. Damage evolution

An important assumption of the model concerns the selection of the internal variables that are used for driving the damage mechanism. The models published in the literature notably differ by the type of coupling between plasticity and damage: plasticity and damage may be driven by the same internal variables or the evolution of these two phenomena may be driven separately using different internal variables. In the latter case, different thresholds are defined for each of these phenomena, which gives flexibility in the modelling as it allows for developing degradation of the elastic properties without developing irreversible strains or vice versa. This approach has been adopted by Wu, et al. (2006) who assume that the evolution of plasticity is driven by the equivalent plastic strains whereas the evolution of damage is driven by the damage energy release rates. In Wu, et al. ’s model, two damage criteria are defined with their damage thresholds, in addition with the yield criteria. However, this approach implies a large number of parameters.

The number of model parameters is reduced by using the same internal variables, and consequently the same threshold, to govern the evolution of plasticity and damage. The models that use a single set of internal variables for driving plasticity and damage make the

implicit assumption that the two phenomena are caused by the same physical mechanisms at the microscopic level. These physical mechanisms at the microscopic level can thus be represented by a single set of macroscopic variables, which are used to model all the phenomenological aspects of the behavior (irreversible strains, degradation of the elastic properties, unilateral effect, etc). The validity of this assumption may be questioned for concrete. Recent investigations by Poinard, et al. (2010) have shown that the concrete behavior can change from a cohesive-brittle behavior governed by damage phenomena at low confinement to that of a granular material governed by plasticity at high confinement; this observation tends to demonstrate that the damage and plastic mechanisms in concrete have different physical origins. Yet, the levels of confinement reached in the considered experiments (higher than 150 N/mm²) are very untypical of structural fire engineering applications. The assumption that the plasticity and damage phenomena in concrete can be driven by the same internal variables has been adopted in several models proposed in the literature (Nechnech, et al., 2002; Grassl and Jirasek, 2006; Matallah and La Borderie, 2009), despite its controversial basis, due to the resulting simplicity of the model and the limited number of parameters. Since it allows to capture the phenomenological behavior of concrete for stress levels typical of structural applications, this approach has been adopted here for its convenience.

In the model, the accumulated plastic strains κ_t and κ_c are the plastic internal variables that drive the yield flow and the hardening process; these variables are also used to drive the evolution of damage. Accordingly, damage is initiated at the same time as permanent strains, and the process of material non-linearity in concrete consists in both damage and plasticity developing simultaneously. Evolution laws are postulated for the damage variables in order to describe the growth of microcracks in the material. Several authors have noted that the damage evolution as a function of the plastic strain is of an exponential form (Lee and Fenves, 1998; Matallah and La Borderie, 2009; de Sa and Benboudjema, 2011); therefore an exponential formulation is adopted here. The evolution laws for tensile and compressive damage as a function of the accumulated plastic strains are given by Eq. (15a) and Eq. (15b), respectively, with a_c a non dimensional model parameter to be determined.

$$d_t\left(\kappa_t\right) = 1 - \left[\frac{1}{2}\exp\left(-a_t\ \kappa_t\right) + \frac{1}{2}\exp\left(-6\,a_t\ \kappa_t\right)\right] \tag{15a}$$

$$d_c\left(\kappa_c\right) = 1 - \exp\left(-a_c\ \kappa_c\right) \tag{15b}$$

Inserting Eq. (13) and Eq. (15a) into the relationship between the effective and the nominal tensile hardening function, it leads to the following expression in the effective stress space: $\bar{\tau}_t\left(\kappa_t\right) = f_t$. The interpretation of this expression is that the softening response of the material in tension is assumed to be driven by the damage mechanism, i.e., it is due to the development of microcracks that progressively reduce the volume of the undamaged material. Consequently, the tensile hardening law in the effective stress space presents a horizontal plateau whereas the experimentally observed softening in concrete is driven by the evolution

of the tensile damage parameter d_t following the damage evolution law of Eq. (15a), see Fig. 4.

In compression, the expressions of Eq. (14) and Eq. (15b) yields the compressive hardening law in the effective stress space. The resulting uniaxial compressive response in the nominal and in the effective stress space is plotted in Fig. 4. As can be seen in Fig. 4, the effective stress-strain response in compression is assumed to exhibit softening due to plastic mechanisms. This assumption is difficult to confirm or refute as separation of softening due to micro-cracking and plasticity in concrete remains an open question. An interesting contribution has been made by Abu Al-Rub and Kim (2010) who have shown, based on the analysis of stress-strain responses under loading-unloading conditions in tension and compression, that the stress-strain response in the effective space does not exhibit softening behavior for these particular loading conditions. Yet, plasticity in concrete is usually interpreted in terms of the friction mechanisms between microcracks surfaces. The friction between two rough microcracks lips leads to an erosion of these surfaces, which results in softening of the shear-slip curve. Based on these physical considerations, the stress-strain response of concrete in compression is expected to exhibit softening; this assumption has also been adopted by Nechnech, et al. (2002).

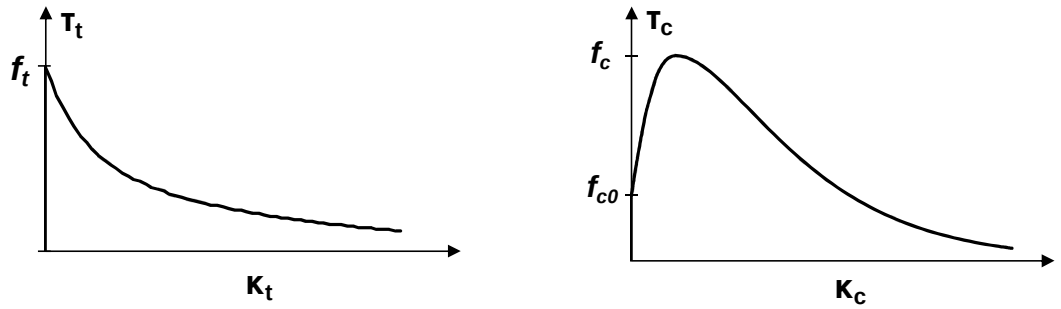

Fig. 3: Hardening laws in the nominal stress space for tension (left) and compression (right)

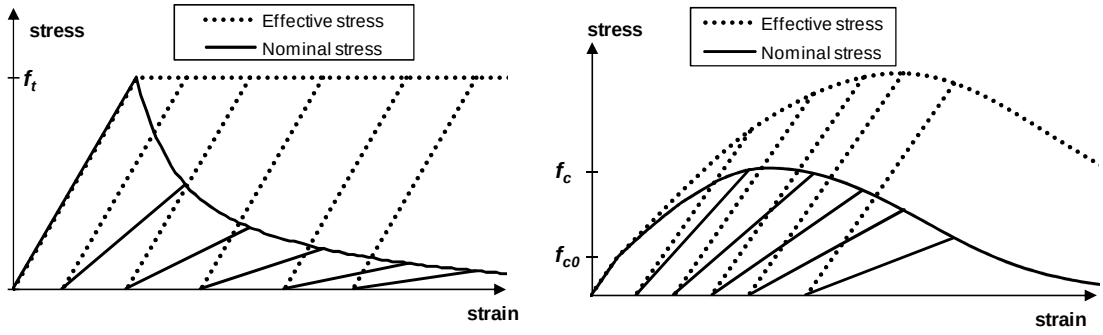

Fig. 4: Uniaxial tensile (left) and compressive (right) response in the effective and nominal stress spaces

2.4. Identification of model parameters

The four non dimensional model parameters a_c, b_c, a_t and κ_{c1} used in the evolution laws of the model can be formulated in terms of material parameters, which can be identified by experimental tests.

The accumulated plastic strain in compression at peak stress, κ_{c1}, can be obtained as a function of the strain ε_{c1} and damage $\tilde{d}_c$ at peak stress under uniaxial compression, and the dilatancy parameter α_g, see Eq. (16). The condition of non negativity of the accumulated plastic strain then leads to a maximum value of 0.50 for the parameter $\tilde{d}_c$, considering the fact that experimental evidence always yields values lower than 1 for the dilatancy parameter α_g in concrete. This condition is in line with experimental observations, as identification from cyclic compression tests (Karsan and Jirsa, 1969) indicates values around 0.30 for the parameter $\tilde{d}_c$.

$$\kappa_{c1} = \frac{\varepsilon_{c1}\left(1-2\,\tilde{d}_c\right)}{\left(2-2\,\tilde{d}_c\right)\left(1-\alpha_g\right)} \tag{16}$$

The parameter a_c that appears in the evolution law for compressive damage can be expressed as a function of the material parameters introduced here above; indeed rewriting of Eq. (15b) at peak stress for uniaxial compression leads to: $a_c = -\ln\left(1-\tilde{d}_c\right)\big/\kappa_{c1}$.

The model parameter a_t that appears in the hardening law in tension is determined based on energetic considerations. As the evolution laws for the hardening variables rely on a work-hardening hypothesis, the total plastic work can be related to the energy dissipation of the material (Feenstra and de Borst, 1996). In tension, the concept of crack energy is often introduced in the constitutive laws for regularization of the model with regards to the mesh sensitivity on the global structural response (Hillerborg, et al., 1976). The concept of equivalent length is also introduced to define a representative dimension of the mesh size in which it is assumed that the crack energy is uniformly dissipated. The total (apparent) plastic work in tension can thus be expressed by Eq. (17), where $\bar{G}_t$ is the crack energy in tension in N.m/m² and l_c is the characteristic length in m also referred to as the localization zone size. The crack energy and the characteristic length are material properties that ensure the objectivity of the numerical simulation at the structural level. However, in the local approach adopted here, the characteristic length is related to the mesh size (Rots, 1988) for regularization of the energy dissipated when strains are localized in a row of finite elements.

$$\int_0^{\infty} \tau_t\left(\kappa_t\right) d\kappa_t = \frac{\bar{G}_t}{l_c} \tag{17}$$

After transformation of Eq. (17), the model parameter a_t can be obtained as a function of the material parameters $\bar{G}_t$, l_c and f_t: $a_t = \left(7\,f_t\,l_c\right)\big/\left(12\bar{G}_t\right)$.

Similar energetic considerations are made for calculation of the parameter of the hardening law in compression b_c. The crack energy in compression $\bar{G}_c$ in N.m/m² is introduced in the constitutive law with the internal length l_c. The total (apparent) plastic work in compression is expressed by Eq. (18).

$$\int_0^{\kappa_{c1}} \tau_c(\kappa_c)\, d\kappa_c + \int_{\kappa_{c1}}^{\kappa_c} \tau_c(\kappa_c)\, d\kappa_c = \frac{\bar{G}_c}{l_c} \tag{18}$$

The left term of the sum in Eq. (18) refers to the crack energy density dissipated before the peak stress, during hardening of the material, whereas the right term of the sum represents the crack energy density dissipated after the peak stress, during softening of the material. This equation allows for expressing the parameter b_c as a function of the material parameters in compression f_c, f_{c0}, $\bar{G}_c$, l_c and κ_{c1}, see Eq. (19). The crack energy $\bar{G}_c$ and internal length l_c can be difficult to derive for practical applications and, if they are not correctly evaluated, Eq. (18) can lead to thermodynamically inconsistent results such as negative dissipation after peak stress. This is avoided by imposing that the total crack energy dissipated at failure be higher than the crack energy dissipated before the peak stress, see Eq. (20).

$$b_c = \frac{2\, f_c}{\left(\bar{G}_c / l_c\right) - \left[\, f_{c0}\, \kappa_{c1} + \left(f_c - f_{c0}\right) \kappa_{c1} \ln 2 \right]} \tag{19}$$

$$\bar{G}_c / l_c > \int_0^{\kappa_{c1}} \tau_c(\kappa_c)\, d\kappa_c \quad \rightarrow \quad \bar{G}_c / l_c > f_{c0}\, \kappa_{c1} + \left(f_c - f_{c0}\right) \kappa_{c1} \ln 2 \tag{20}$$

2.5. Material parameters

The ten material parameters contained in the model are summarized in Table 1. These parameters can be obtained by three tests at ambient temperature: uniaxial compression test until failure comprising one unloading-reloading at peak stress, biaxial compression test until peak stress, and uniaxial tension test until failure. It is noted that the elastic modulus is not an independent parameter in the model and therefore it does not appear in Table 1; the elastic modulus is calculated from the uniaxial compressive strength and the peak stress strain.

In addition, the characteristic length l_c has to be defined as a function of the model. This characteristic length depends on the chosen element type, element size, element shape and integration scheme (Feenstra and de Borst, 1996). A very simple formula has been proposed for biaxial cases (Rots, 1988), see Eq. (21). In this equation, A_e is the area of the element and α_l is a modification factor which is equal to 1 for quadratic elements and equal to $\sqrt{2}$ for linear elements. This formula gives good approximation for most practical applications.

$$l_c = \alpha_l . \sqrt{A_e} \tag{21}$$

Fig. 5 presents the effect of the material parameter $\tilde{d}_c$ on the unloading response in a uniaxial compression test, next to experimental data (Karsan and Jirsa, 1969). This parameter allows for controlling the relative importance of the damage process with respect to the plastic process in the model. For low values of this parameter, the plastic process prevails over the damage process in compression, which results in significant development of plastic strains and relatively limited degradation of the elastic properties. On the contrary, for high values of this parameter (but lower than 0.50) the response is mostly driven by the damage process. Based on these experimental data, it is found that the value for the compressive damage at peak stress is around 0.30.

Symbol	Parameter	Units	Required test
ν	Poisson's ratio	[−]	Uniaxial compression
f_{c0}	Compr. limit of elasticity	[N/m²]	Uniaxial compression
f_c	Uniaxial compr. strength	[N/m²]	Uniaxial compression
ε_{c1}	Peak stress strain	[−]	Uniaxial compression
α_g	Dilatancy parameter	[−]	Uniaxial compression
$\bar{G}_c$	Compr. crack energy	[Nm/m²]	Uniaxial compression
$\tilde{d}_c$	Compr. damage at peak stress	[−]	Uniax. compr. + unloading
f_b	Biaxial compr. strength	[N/m²]	Biaxial compression
f_t	Uniaxial tensile strength	[N/m²]	Uniaxial tension
$\bar{G}_t$	Tensile crack energy	[Nm/m²]	Uniaxial tension

Table 1: Material parameters in the concrete model

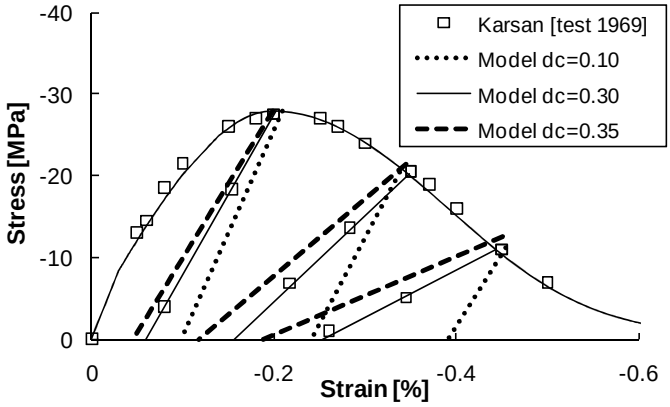

Fig. 5: Identification of the model parameter $\tilde{d}_c$ in a uniaxial compression test

3 Extension to high temperatures

The division of the total strain tensor into individual strain components according to Eq. (1) has been adopted in the present model. In Section 2, a plastic-damage model has been developed for capturing the relationship between the instantaneous stress related strain tensor $\underline{\underline{\varepsilon}}_\sigma$ and the stress tensor $\underline{\underline{\sigma}}$ at ambient temperature. Section 3 presents the extension of this

model to high temperatures and the relationships for calculation of the free thermal strain tensor $\underline{\underline{\varepsilon}}_{th}$ and the transient creep strain tensor $\underline{\underline{\varepsilon}}_{tr}$ under multiaxial stress states.

3.1. Free thermal strain

The relationship for calculation of the free thermal strain in multiaxial stress state is adapted from the uniaxial relationship of Eurocode 2 (2004-a). This latter relationship gives the free thermal strain as a nonlinear function of temperature that depends on the type of aggregate (siliceous or calcareous), see Eq. (22a-b). The expression is generalized to the multiaxial stress state using the assumption of isotropy: $\underline{\underline{\varepsilon}}_{th}(T) = \varepsilon_{th,EC2}(T) \times \underline{\underline{I}}$, in which $\underline{\underline{I}}$ is the second order identity tensor and $\varepsilon_{th,EC2}(T)$ is the free thermal strain given by Eurocode 2.

$$\begin{aligned} &\varepsilon_{th}(T) = -1.8\times10^{-4} + 9\times10^{-6}\,T + 2.3\times10^{-11}\,T^3 \quad ; 20°C \le T \le 700°C \\ &\varepsilon_{th}(T) = 14\times10^{-3} \qquad\qquad\qquad\qquad\qquad\qquad\quad ; 700°C < T \le 1200°C \end{aligned} \tag{22a}$$

$$\begin{aligned} &\varepsilon_{th}(T) = -1.2\times10^{-4} + 6\times10^{-6}\,T + 1.4\times10^{-11}\,T^3 \quad ; 20°C \le T \le 805°C \\ &\varepsilon_{th}(T) = 12\times10^{-3} \qquad\qquad\qquad\qquad\qquad\qquad\quad ; 805°C < T \le 1200°C \end{aligned} \tag{22b}$$

The free thermal strain of concrete is partly irreversible (Schneider, 1988; Franssen, 1993); a residual dilatation or residual contraction is observed after cooling down to ambient temperature depending on the maximum temperature reached in the material. This irreversibility is taken into account in the model; the value of the residual free thermal strain as a function of the maximum temperature is taken from experimental tests made by Schneider (1988).

3.2. Transient creep strain

The model for calculation of transient creep strain is adapted from the Explicit Transient Creep (ETC) Eurocode model, developed at University of Liege for uniaxial relationships (Gernay and Franssen, 2010; Gernay and Franssen, 2012). This ETC model, which includes an explicit term for transient creep strain, is built as a generalization of the current Eurocode concrete model. Whereas the Eurocode implicit model had been developed for prescriptive design, the ETC model is able to compute accurately the transient creep strain that develops in performance-based situations, which may include cooling phases or load redistributions (Gernay, 2012-a). Meanwhile, the ETC model remains generic and it yields the same results as the Eurocode model in the simple prescriptive situations, which is an advantage to the authors' opinion as the Eurocode model has been widely used in the last decades and is well accepted by authorities and regulators for building design.

Generalization of the transient creep strain formula to a multiaxial stress state is based on the assumption that the process of transient creep does not induce anisotropy. The formulation proposed by de Borst and Peeters (1989), which has been widely adopted in the literature (Khennane and Baker, 1992; Nechnech, et al., 2002; Gawin, et al., 2004; de Sa and

Benboudjema, 2011), is used here and applied to the ETC model, see Eq. (23). In this equation, $\underline{\underline{\dot{\varepsilon}}}_{tr}$ is the rate of the transient creep strain tensor, $\dot{\phi}(T)$ is the rate of the transient creep function which values are given in Table 2, $\underline{\underline{\bar{\sigma}}}^{-}$ is the negative part of the effective stress tensor, $f_{c,20}$ is the compressive strength at 20°C and $\underline{\underline{\underline{\underline{H}}}}$ is the fourth order tensor given by $H_{ijkl} = -\gamma \delta_{ij} \delta_{kl} + 0.5(1+\gamma)\left(\delta_{ik} \delta_{jl} + \delta_{il} \delta_{jk}\right)$. The material parameter γ that appears in this latter expression can be taken equal to Poisson's ratio (Nechnech, et al., 2002), in accordance with Thelandersson's multiaxial data (1987), whereas δ_{ij} is the Kronecker symbol.

$$\underline{\underline{\dot{\varepsilon}}}_{tr} = \dot{\phi}(T)\, \underline{\underline{\underline{\underline{H}}}} : \frac{\underline{\underline{\bar{\sigma}}}^{-}}{f_{c,20}} \tag{23}$$

T [°C]	20	100	200	300	400	500	600	700	800
Silic.	0.0000	0.0010	0.0018	0.0024	0.0049	0.0106	0.0274	0.0389	0.0733
Calc.	0.0000	0.0010	0.0017	0.0022	0.0043	0.0086	0.0206	0.0271	0.0407

Table 2: Transient creep function *Φ(T)* for siliceous and calcareous aggregates concrete.

The particularity of the formulation of Eq. (23) is that the calculation of the transient creep strain rate tensor is based on the negative part of the effective stress tensor. In models in which damage develops, it is consistent to use the effective stress rather than the nominal stress for calculation of transient creep strain because it can be assumed that the mechanism of transient creep occurs in the undamaged part of the material. In addition, it has been assumed in the ETC model that transient creep develops under compressive stress only; for this reason only the negative part of the effective stress tensor is considered in Eq. (23).

After integration over a finite time step, and adopting an explicit numerical scheme, the transient creep strain tensor can be computed using Eq. (24). Computation of the transient creep strain increment takes into account the stress-temperature history. Between step *(s+1)* and *(s)*, there is an increment in transient creep strain, which value is computed by Eq. (24), if and only if the three following conditions are fulfilled:

i. The temperature at time step *(s+1)* exceeds the maximum temperature reached previously in the history of the material;
ii. The negative part of the (converged) effective stress at time *(s)* is non-null (material subjected to compressive stress);
iii. The material is in the ascending branch of the constitutive relationship, i.e. $\kappa_c \leq \kappa_{c1}$.

It is assumed that the transient creep strain is irreversible at both load and temperature decrease.

$$\underline{\underline{\varepsilon}}_{tr}^{(s+1)} = \underline{\underline{\varepsilon}}_{tr}^{(s)} + \left[\phi\left(T^{(s+1)}\right) - \phi\left(T^{(s)}\right)\right] \left[\underline{\underline{\underline{\underline{H}}}} : \frac{\left(\bar{\underline{\underline{\sigma}}}^{-}\right)^{(s)}}{f_{c,20}}\right] \tag{24}$$

3.3. Temperature-dependency of the material parameters

Concrete subjected to elevated temperatures exhibits thermo-mechanical degradation of its properties of strength and stiffness; this effect is taken into account through proper temperature dependency of the material parameters. The evolution laws of the parameters with temperature are taken from design codes such as Eurocode 2, when available, or from experimental data published in the literature.

The evolution of the uniaxial tensile and compressive strengths $f_{t,T}$ and $f_{c,T}$ with temperature is taken from Eurocode 2. Evolution of these parameters with temperature results in a modification of the yield surfaces; these surfaces experience isotropic contraction at high temperature due to the decrease of the hardening functions caused by the decrease of the strengths.

Compressive strength of concrete does not recover during cooling. According to Eurocode 4 part 1-2 (2004-b), an additional loss of 10% in compressive strength is considered during cooling from maximum to ambient temperature. This assumption prescribed by the Eurocode has been recently confirmed by an analysis based on hundreds of experimental results reported in the literature (Li and Franssen, 2011), where it was shown that the additional reduction during cooling may be even higher than the 10% reduction considered in Eurocode 4. In fact, the residual strength of concrete after fire exposure depends on many parameters (Annerel, 2010) and its proper evaluation would probably require a more advanced model taking into account the effect of the different parameters, but the Eurocode formula has been adopted here because of its simplicity and its generic form and because it has the advantage of being a standard code formula. Consideration of the additional loss in compressive strength during cooling is of prime importance in the analysis of structures subjected to natural fire. Recent research based on numerical simulations have highlighted the possibility of collapse of reinforced concrete columns during or even after the cooling phase of a fire and one of the main mechanisms that lead to this type of failure is the additional loss of concrete strength during the cooling phase of the fire (Dimia, et al., 2011; Gernay and Dimia, 2011).

The peak stress strain in uniaxial compression ε_{c1} increases with temperature, see Table 3. The value of the peak stress strain has been defined such that, for a concrete specimen subjected to heating under constant uniaxial compressive stress (situation of transient test), the new concrete model yields the same response as the current Eurocode 2 model (Gernay and Franssen, 2012). During cooling, the peak-stress strain is considered as fixed to the value that prevailed at the maximum temperature, according to Eurocode 4.

T [°C]	20	100	200	300	400	500	600	700	800
ε_{c1} [-]	0.0025	0.0030	0.0038	0.0050	0.0063	0.0087	0.0127	0.0133	0.0140

Table 3: Evolution of the peak stress strain in uniaxial compression with temperature.

A dependency of Poisson's ratio with temperature has been experimentally observed by different authors (Maréchal, 1970 cited in Schneider, 1985; Luccioni, et al., 2003). This temperature-dependency has been approximated by the bilinear relationship of Eq. (25) in the model. The transition temperature T_ν is equal to 500°C.

$$\begin{aligned} \nu(T) &= \nu_{20}\left(0.2+0.8\times\frac{T_\nu - T}{T_\nu - 20}\right) \quad ; \quad T \le T_\nu \\ \nu(T) &= 0.2\times\nu_{20} \quad ; \quad T > T_\nu \end{aligned} \tag{25}$$

Experimental results indicate that the confinement effect is more pronounced in heated concrete because elevated temperatures cause the degradation of the micro-structure and an increase in porosity. As a result, at a given temperature the decrease in biaxial compressive strength $f_{b,T}$ is smaller than the decrease in uniaxial compressive strength $f_{c,T}$. Based on the experimental results by Ehm and Schneider (1985), the ratio between these two parameters $\beta(T) = f_{b,T} / f_{c,T}$, equal to 1.16 at ambient temperature, is calculated using the formula of Eq. (26) at high temperature. The transitions temperature $T_{\beta 1}$ and $T_{\beta 2}$ are respectively equal to 350°C and 750°C.

$$\begin{aligned} \beta(T) &= 1.16 \quad ; \quad T \le T_{\beta 1} \\ \beta(T) &= 1.16\left(1+0.6\times\left(\frac{T - T_{\beta 1}}{T_{\beta 2} - T_{\beta 1}}\right)\right) \quad ; \quad T_{\beta 1} < T \le T_{\beta 2} \\ \beta(T) &= 1.86 \quad ; \quad T_{\beta 2} < T \end{aligned} \tag{26}$$

Due to a lack of experimental data, it is difficult to assess the temperature-dependency of the other parameters; therefore, simplifying assumptions have been adopted. It is assumed that the approximately linear elastic concrete response in uniaxial compression for low stress levels remains proportionally unchanged at high temperature, i.e. the ratio between the compressive limit of elasticity $f_{c0,T}$ and the uniaxial compressive strength $f_{c,T}$ at high temperature is considered constant. It is also assumed that the plastic potential in compression G_c experiences isotropic contraction at high temperature with no modification in its shape; therefore the dilatancy parameter α_g does not vary with temperature. Based on similar considerations, the compressive damage at peak stress $\tilde{d}_c$ has been considered as constant with temperature. For the crack energy in compression, it has been assumed that the ratio between the crack energy dissipated before the peak stress and the total crack energy dissipated at failure $\bar{G}_c$ remains constant with temperature. As the former is defined from other material parameters, this assumption yields to a unequivocal definition of the temperature dependency of $\bar{G}_c$. Finally, different authors have tried to quantify the

temperature dependency of the tensile crack energy $\bar{G}_t(T)$ but experimental results show a significant scatter depending on the test specimens and test methods, so that it is difficult to derive a reliable model for the temperature dependency of this parameter. As this energy parameter can be related to the area under the tensile softening function curve, it should be related to the uniaxial tensile strength $f_{t,T}$. In particular for temperatures beyond 600°C, $f_{t,T}$ is equal to 0 and therefore the tensile crack energy parameters $\bar{G}_t$ must also be equal to 0. By convenience, it was assumed that the tensile crack energy $\bar{G}_t$ follows the same temperature dependency as the uniaxial tensile strength.

4 Numerical implementation

The model has been implemented within the framework of the nonlinear finite element method. The numerical implementation deals with the case of fully tridimensional stress states as well as plane stress states.

For the local problem, it is assumed that at time step s the finite element code has converged, i.e. the values of the strains, stresses and internal variables are known at every integration point. The values of the displacements at the nodes are also defined. Then, from time step s to time step $s+1$, the variation of the displacements of the nodes calculated by the finite element code produces an increment in total strain. The problem is then to update the basic variables describing the local state of the material in a manner that is consistent with the constitutive law. This process should also yield the tangent modulus of the constitutive law, to be used by the finite element code in the global iteration process.

It is assumed that the temperatures are known in all integration points, as a result of the thermal analysis that has been performed before the mechanical analysis.

First, the mechanical properties, the free thermal strain $\underline{\underline{\varepsilon}}_{th}^{(s+1)}$ and the transient creep strain $\underline{\underline{\varepsilon}}_{tr}^{(s+1)}$ are computed at time step $s+1$, for all integration points. This computation takes into account the temperatures at time step $s+1$, according to the relationships defined in Section 3.

Then, the free thermal strain and the transient creep strain are subtracted to the total strain to yield the instantaneous stress-related strain. As the resolution of the equilibrium in the structure at a given time step is an iterative process, the increment in total strain produced by the finite element code is updated several times at each time step. The increment in total strain from converged time step s to iteration $i+1$ of time step $s+1$ is noted $\Delta\underline{\underline{\varepsilon}}_{tot}$ and the total strain at iteration $i+1$ of time step $s+1$ is given by: $\underline{\underline{\varepsilon}}_{tot}^{(i+1)} = \underline{\underline{\varepsilon}}_{tot}^{(s)} + \Delta\underline{\underline{\varepsilon}}_{tot}$. Yet, the free thermal strain and the transient creep strain do not vary during the iteration process; they are only computed once at the beginning of the procedure, before entering into the iterative resolution of the equilibrium at the considered time step. At iteration $i+1$, the instantaneous stress-related strain vector can thus be computed using Eq. (27).

$$\underline{\underline{\varepsilon}}_{\sigma}^{(i+1)} = \underline{\underline{\varepsilon}}_{tot}^{(i+1)} - \underline{\underline{\varepsilon}}_{th}^{(s+1)} - \underline{\underline{\varepsilon}}_{tr}^{(s+1)} \tag{27}$$

At each iteration, solving the local problem consists in finding the updated values of the stresses, the updated values of the internal variables and the tangent modulus corresponding to the instantaneous stress-related strain vector of Eq. (27), for all integration points. As this operation requires an iterative process, there is a second level of iterations in the general algorithm, referred to as “internal iterations” in the following.

The constitutive relationship of Eq. (3) leads to Eq. (28) for the calculation of the stress at iteration $i+1$ of time step $s+1$.

$$\underline{\underline{\sigma}}^{(i+1)} = \left(\underline{\underline{\underline{\underline{I}}}} - \underline{\underline{\underline{\underline{D}}}}^{(i+1)} \right) : \underline{\underline{\underline{\underline{C}}}}_0 : \left(\underline{\underline{\varepsilon}}_{\sigma}^{(i+1)} - \underline{\underline{\varepsilon}}_p^{(i+1)} \right) \tag{28}$$

The computation of the stress from the instantaneous stress-related strain using Eq. (28) is decomposed into three parts in the numerical algorithm according to the concept of operator split (Simo and Hughes, 1998), i.e. into the computation of an elastic predictor, plastic corrector and damage corrector. Among the three parts of the algorithm, only the computation of the plastic corrector is an iterative process. As the damage variables are fixed during the elastic predictor and the plastic corrector steps, solving of these two steps constitutes a standard elastoplastic problem in the effective stress space. Then, computation of the damage variables is an explicit operation as these variables are driven by the plastic internal variables.

The computation of the elastic predictor and the plastic corrector in the effective stress space are detailed herein. The effective stress $\underline{\underline{\bar{\sigma}}}^{(i+1)}$, the plastic strain $\underline{\underline{\varepsilon}}_p^{(i+1)}$ and the plastic hardening variables κ_t, κ_c (equivalent to the plastic multipliers λ_t, λ_c) must satisfy the stress-strain equation of Eq. (29), the incremental Kuhn-Tucker conditions of Eq. (30) and the discretized form of the evolution laws (Eq. (31) and Eq. (32)).

$$\underline{\underline{\bar{\sigma}}}^{(i+1)} = \underline{\underline{\underline{\underline{C}}}}_0 : \left(\underline{\underline{\varepsilon}}_{\sigma}^{(i+1)} - \underline{\underline{\varepsilon}}_p^{(i+1)} \right) \tag{29}$$

$$\Delta\lambda_j \geq 0\,, \quad F_j\left(\underline{\underline{\bar{\sigma}}}, \kappa_j\right) \leq 0\,, \quad \Delta\lambda_j \, F_j\left(\underline{\underline{\bar{\sigma}}}, \kappa_j\right) = 0 \quad \big| \quad j = t, c \tag{30}$$

$$\underline{\underline{\varepsilon}}_p^{(i+1)} = \underline{\underline{\varepsilon}}_p^{(s)} + \Delta\lambda_t \frac{\partial G_t}{\partial \underline{\underline{\bar{\sigma}}}} + \Delta\lambda_c \frac{\partial G_c}{\partial \underline{\underline{\bar{\sigma}}}} \tag{31}$$

$$\kappa_t^{(i+1)} = \kappa_t^{(s)} + \Delta\lambda_t \geq 0\,, \quad \kappa_c^{(i+1)} = \kappa_c^{(s)} + \Delta\lambda_c \geq 0 \tag{32}$$

The trial elastic effective stress (elastic predictor) is first computed from the instantaneous stress-related strain increment using Eq. (33). It is checked whether this stress state is acceptable by inserting $\underline{\underline{\bar{\sigma}}}^{tr(i+1)}$, $\Delta\lambda_t = 0$ and $\Delta\lambda_c = 0$ into the Kuhn-Tucker conditions of Eq. (30). If these conditions are satisfied, i.e. if the trial stress is not outside the yield surfaces, the step is elastic and there is no variation in the plastic internal variables. The updated variables at iteration $i+1$ of time step $s+1$ are then given by Eq. (34). As the plastic internal variables govern the evolution laws of the model, there is no variation in the plastic strains neither in the damage variables.

$$\underline{\underline{\bar{\sigma}}}^{tr(i+1)} = \underline{\underline{\underline{\underline{C}}}}_0 : \left(\underline{\underline{\varepsilon}}_{\sigma}^{(i+1)} - \underline{\underline{\varepsilon}}_{p}^{(s)} \right) = \underline{\underline{\bar{\sigma}}}^{(s)} + \underline{\underline{\underline{\underline{C}}}}_0 : \Delta \underline{\underline{\varepsilon}}_{\sigma} \tag{33}$$

$$\underline{\underline{\varepsilon}}_{p}^{(i+1)} = \underline{\underline{\varepsilon}}_{p}^{(s)} \; ; \quad \kappa_t^{(i+1)} = \kappa_t^{(s)} \; ; \quad \kappa_c^{(i+1)} = \kappa_c^{(s)} \; ; \quad \underline{\underline{\bar{\sigma}}}^{(i+1)} = \underline{\underline{\bar{\sigma}}}^{tr(i+1)} \tag{34}$$

Yet, if the Kuhn-Tucker conditions are not satisfied in the elastic predictor stress state, plastic strains develop in the material between time step *s* and (iteration *i+1* of) time step *s+1*. The effective stress vector has to be corrected by a plastic corrector according to Eq. (35) to return on the yield surface.

$$\underline{\underline{\bar{\sigma}}}^{(i+1)} = \underline{\underline{\bar{\sigma}}}^{tr(i+1)} - \underline{\underline{\underline{\underline{C}}}}_0 : \Delta \underline{\underline{\varepsilon}}_{p} \tag{35}$$

The plastic strain increment $\Delta \underline{\underline{\varepsilon}}_{p}$ can be eliminated from the problem by substituting Eq. (31) into Eq. (35), which leads to the expression of Eq. (36).

$$\underline{\underline{\bar{\sigma}}}^{(i+1)} = \underline{\underline{\bar{\sigma}}}^{tr(i+1)} - \underline{\underline{\underline{\underline{C}}}}_0 : \left(\Delta\lambda_t \frac{\partial G_t \left(\underline{\underline{\bar{\sigma}}}^{(i+1)} \right)}{\partial \underline{\underline{\bar{\sigma}}}} + \Delta\lambda_c \frac{\partial G_c \left(\underline{\underline{\bar{\sigma}}}^{(i+1)} \right)}{\partial \underline{\underline{\bar{\sigma}}}} \right) \tag{36}$$

The set of nonlinear equations can finally be rewritten as a function of the plastic multipliers $\{\Delta\lambda_t, \Delta\lambda_c\}$ using Eq. (32) for the hardening parameters and Eq. (36) for the effective stress. By applying an implicit backward Euler difference scheme, the problem is transformed into a constrained-optimization problem governed by discrete Kuhn-Tucker conditions, with the plastic multipliers $\{\Delta\lambda_t, \Delta\lambda_c\}$ as the two unknowns in Eq. (30).

Solving of the system of equations is performed using a Newton iterative process. In multi-surface plasticity, the fact that a yield surface is ultimately active (at convergence) cannot be guaranteed in advance based on the trial elastic state. By definition, a yield surface F_j is termed active if $\Delta\lambda_j > 0$. The initial set of active yield surfaces is determined in the trial elastic state by the condition $F_j \left(\underline{\underline{\bar{\sigma}}}^{tr(i+1)}, \kappa_j^{(s)} \right) > 0$. However, this initial configuration cannot provide a sufficient criterion for determining which surface is active at the end of the time step because the final location of the yield surfaces and the final location of their intersection are unknown at the beginning of the time step. Therefore, the set of active yield surfaces has to be updated during the iterative resolution of the system. As softening plasticity is considered here, a yield surface that was inactive in the trial elastic state can be activated during the return-mapping (Pramono and Willam, 1989; Feenstra and de Borst, 1996). A condition is therefore implemented in the iterative process for re-activation of yield surface F_j at iteration $n+1$ if $\Delta\lambda_j^{(n+1)}$ has become positive. On the opposite, yield surface F_j is deactivated at iteration $n+1$ if $\Delta\lambda_j^{(n+1)}$ has become negative. The details of the solving process are given in (Gernay, 2012-b).

Finally, application of the Newton algorithm yields the updated values of the plastic multipliers $\Delta\lambda_t$ and $\Delta\lambda_c$ at iteration $i+1$ of time step $s+1$. As a result, the plastic corrector step can be applied by updating the effective stress, the plastic strain and the plastic internal

variables using Eq. (36), Eq. (31) and Eq. (32), respectively. It remains then to update the damage variables and to apply the damage corrector to the stress tensor.

The computation of the tensile and the compressive damage variables at iteration $i+1$ of time step $s+1$ is explicitly performed as a function of the plastic internal variables $\kappa_t^{(i+1)}$ and $\kappa_c^{(i+1)}$. The tensile damage variable is computed using Eq. (37). As it has been assumed in Section 3.3 that the temperature dependency of f_t and $\bar{G}_t/l_c$ is the same, the parameter a_t does not depend on temperature and remains constant at each time step.

$$d_t^{(i+1)} = 1 - \left[\frac{1}{2} \exp\left(-a_t \, \kappa_t^{(i+1)}\right) + \frac{1}{2} \exp\left(-6 \, a_t \, \kappa_t^{(i+1)}\right) \right] \tag{37}$$

The compressive damage variable is computed using Eq. (38). The model parameter $a_c^{(s+1)}$ that appears in this equation depends on temperature and therefore it is calculated at each time step when the mechanical properties at temperature $T^{(s+1)}$ are evaluated.

$$d_c^{(i+1)} = 1 - \exp\left(\ln\left(1 - d_c^{(s)}\right) - a_c^{(s+1)} \left(\kappa_c^{(i+1)} - \kappa_c^{(s)} \right) \right) \tag{38}$$

The updated damage tensor is computed using Eq. (39), where the projection tensors apply to the effective stress $\underline{\underline{\bar{\sigma}}}^{(i+1)}$ at iteration $i+1$ of time step $s+1$. Finally, the nominal stress is calculated using Eq. (40).

$$\underline{\underline{\underline{\underline{D}}}}^{(i+1)} = d_t^{(i+1)} \, \underline{\underline{\underline{\underline{P}}}}^{+} + d_c^{(i+1)} \, \underline{\underline{\underline{\underline{P}}}}^{-} \tag{39}$$

$$\underline{\underline{\sigma}}^{(i+1)} = \left(\underline{\underline{\underline{\underline{I}}}} - \underline{\underline{\underline{\underline{D}}}}^{(i+1)} \right) \cdot \underline{\underline{\underline{\underline{C}}}}_0 \cdot \left(\underline{\underline{\varepsilon}}_{\sigma}^{(i+1)} - \underline{\underline{\varepsilon}}_{p}^{(i+1)} \right) \tag{40}$$

The Newton-Raphson method is used in the global iteration process for solving the equilibrium of the structure. This method is based on the estimation of a tangent stiffness matrix, which is built for the structure from the operators linking the increment of stress to the linearized increment of strain at each integration point. These operators are computed for all integration points once the processes of plastic-corrector and damage-corrector have been performed, i.e. at the end of the process of internal iterations. The developments leading to the expression of these operators, which are written in the nominal stress space and are derived consistently with the algorithm for updating the nominal stress, can be found in (Gernay, 2012-b).

As the concrete model is developed as fully tridimensional, it can be used with three-dimensional solid finite elements. However in many applications of structural engineering, it is interesting to use finite elements that develop plane stress states. Basically, two strategies can be adopted to obtain a plane stress constitutive model from a fully three-dimensional model. First, the model can be rewritten considering a plane stress state. The advantage of this method is that several simplifications can be made in the equations of the model and its numerical implementation due to the consideration of a plane stress state. However, the entire model has to be rewritten and implemented separately in the numerical code, which represents a considerable amount of work and leads to the necessity for the developer to handle two

distinct models in parallel. The second strategy consists in implementing an additional piece of numerical code in the algorithm of the fully three-dimensional model to deal with the particular case of plane stress. The advantage of this method is its consistency as a single material model is used for the three-dimensional stress states and plane stress states. The disadvantage of this method is the fact that no benefit is taken in terms of CPU time from the fact that the stress state is simplified to a plane stress state. This second strategy is chosen here in order to avoid rewriting a different model for plane stress states. The numerical code developed by Charras (2010, implemented in the finite elements software CAST3M, 2003), which relies on the implementation of an additional constraint in the return mapping algorithm to find the particular solution corresponding to plane stress state, has been adopted in this work.

5 Validation of the model based on experimental tests on concrete samples

In this section, the model is tested by comparison against experimental data of concrete samples subjected to various situations of applied stress and/or temperature. To focus on the concrete constitutive model, the numerical simulations are conducted using a single cube-shaped three-dimensional finite element made of eight nodes. During the simulations, it is verified that all the integration points in this finite element have the same stress-strain response. The numerical simulations are performed with the software SAFIR (Franssen, 2005), which allows to verify the correct implementation of the concrete model in this software. Numerical simulations of structural elements will be conducted in a forthcoming paper.

	Uniaxial comp.	Uniaxial tension	Bicomp. (ambient)	Tricomp. (Imran)	Tricomp. (Poinard)	Transient test	Bicomp. (hot)
$f_c\,[\mathrm{N/mm^2}]$	33.0	-	30.0	28.6	40.0	30	41
$f_{c0}/f_c\,[-]$	0.30	-	0.30	0.30	0.30	0.30	0.30
$\varepsilon_{c1}\,[\%]$	0.21	-	0.25	0.25	0.25	0.25	0.25
$\tilde{d}_c\,[-]$	0.25	-	0.30	0.30	0.30	0.30	0.30
$\bar{G}_c\,[\mathrm{N.mm/mm^2}]$	15.1	-	18.7	21.4	15.7	11.8	16.1
$\upsilon\,[-]$	0.18	-	0.20	0.20	0.20	0.20	0.20
$\alpha_g\,[-]$	0.25	-	0.25	0.25	0.25	0.25	0.25
$f_t\,[\mathrm{N/mm^2}]$	-	3.5	-	-	-	-	-
$\bar{G}_t\,[\mathrm{N.mm/mm^2}]$	-	0.045	-	-	-	-	-
$f_b/f_c\,[-]$	-	-	1.16	1.16	1.16	1.16	1.16

Table 4: Values of the material parameters.

The values of the material parameters used in the numerical simulations are given in Table 4; these values are obtained by calibration of the numerical response on the

experimental behavior. The side dimension of the finite elements used in the model is 0.10 m; hence, the characteristic length is taken equal to 0.10 m, based on Eq. (21). The values of the compressive crack energy range between 11.8 and 21.4 N.mm/mm², which is consistent with the values given by Vonk (1992).

5.1. At ambient temperature

The concrete model is first tested in uniaxial compression at ambient temperature. In the test, one side of the concrete sample is subjected to increasing negative displacement in one direction whereas the two perpendicular directions are free. The numerical results are compared with the experimental results by Kupfer, et al. (1969) (see Fig. 6) which include data of the volumetric strains. A value of 0.25 for the dilatancy parameter α_g allows for capturing properly the volumetric behavior of the material.

In uniaxial tension, the numerical results obtained with the new concrete model are compared with experimental results by Gopalaratnam and Shah (1985) in Fig. 7. The computed results have been obtained using a tensile crack energy $G_t = 0.045$ N.mm/mm². Application of the CEB formula (CEB-FIB, 1990) for the evaluation of the crack energy in tension $\bar{G}_t$ typically leads to values between 0.050-0.150 N.mm/mm².

The concrete model captures the experimentally observed unilateral effect, characterized by a stiffness recovery due to closure of tensile cracks, as shown in Fig. 1. Full stiffness recovery is assumed when moving from tension to compression. Indeed, in the model, the tensile damage scalar is directly multiplied by the positive part of the effective stress tensor. Lee and Fenves (1998) have suggested introducing an additional parameter to set a minimum value to the factor multiplying the tensile damage scalar when the positive part of the stress becomes null, in order to account for partial stiffness recovery. This approach has not been adopted here for minimization of the number of parameters and because of reasonably good agreement with experimental results (Fig. 1).

Fig. 8 shows the model response in case of cyclic uniaxial compressive-tensile loading. After crushing in compression, the concrete is unloaded into tension. Due to tensile loading beyond the concrete tensile strength, a tensile crack develops. When the sample is reloaded in compression, the crack is first partially closed before the stress comes back to compression; yet, it can be noted that plastic strains also develop in tension and consequently, the reloading in compression is slightly shifted from the unloading path, which indicates a plastic dissipation during the cycle. The material response then returns on the (shifted) softening branch in compression. A second cycle of uniaxial compression-tension-compression is finally performed, showing the same phenomena as the first cycle.

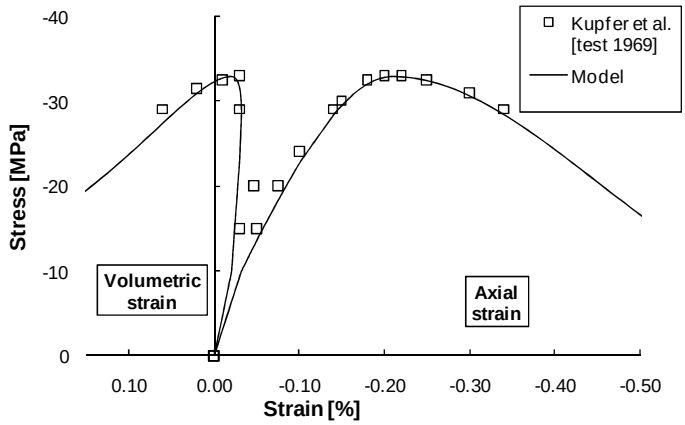

Fig. 6: Measured and computed results for concrete in uniaxial compression.

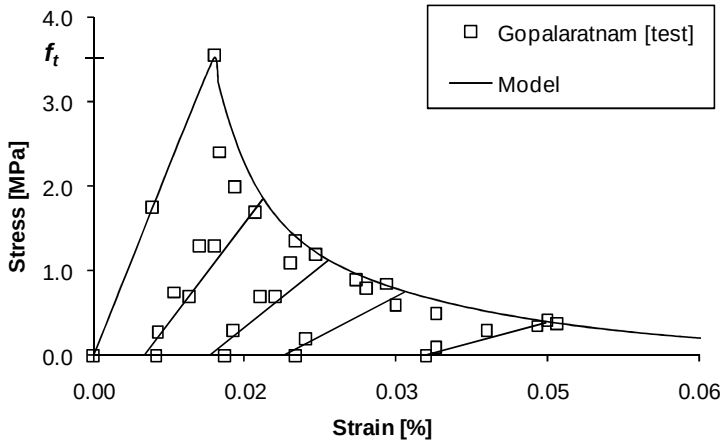

Fig. 7: Measured and computed results for concrete in uniaxial tension.

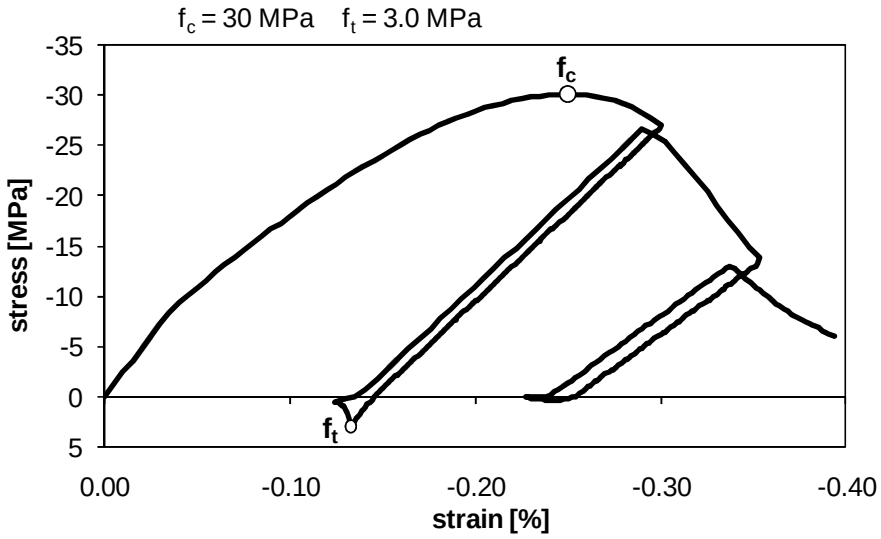

Fig. 8: Model response under uniaxial compression-tension-compression load sequences

Concrete is a pressure-sensitive material which exhibits increase in strength and ductility under multiaxial compression, as compared to uniaxial compression. The ability of the model to capture this behavior is verified by comparison against experimental data by Kupfer, et al. (1969), see Fig. 9. These tests are also used to calibrate the biaxial compressive strength parameter $\beta_{20} = f_b / f_c$. Proper estimation of the increase in strength due to the confinement effect in biaxial compression is obtained for a value of 1.16 for this latter parameter; this value is typically found in the literature (Grassl and Jirasek, 2006).

Finally, the concrete behavior under triaxial compression has been investigated. In the three tests of Fig. 10, the concrete, which has a uniaxial compressive strength of 28.6 N/mm², was subjected to hydrostatic stress of 2.1 N/mm², 8.4 N/mm² and 21 N/mm² respectively, and then to increasing deviatoric stress in one direction until failure (Imran, 1994). It is observed that the concrete strength and ductility increase with confinement; for significant confinement the behavior becomes highly ductile. The model qualitatively captures the increase of strength with increasing level of confinement but this strength increase is underestimated by the model. Similarly, the model predicts an increase in ductility with increasing level of confinement but this effect is not as pronounced as experimentally observed.

In fact, the model is relatively good at capturing the experimental response until it reaches the model peak stress. The increase in stiffness at the different levels of confinement is quite accurately modeled, as well as the pre-peak evolution of the transversal strains ε_1 and ε_2. The relationship between the stress and the strain in the direction of the applied deviatoric stress is also relatively well assessed until approximately $\varepsilon_3 = \varepsilon_{c1}$. Then, the model reaches a peak stress and the computed results beyond this level of strain significantly differ from the experimental results. The experimental results show that the post-peak behavior of concrete changes from softening to hardening behavior with increasing level of confinement, whereas this effect is not represented in the model and the post-peak behavior remains a softening behavior in the simulations of the three tests. At 2.1 N/mm² confinement ($=0.07\times f_c$), the experimental response exhibits softening and the computed response reasonably agree with the experimental response. However at 8.4 N/mm² confinement ($=0.29\times f_c$), the experimental response exhibits hardening and, as the model fails at reproducing this effect, the computed response stops being accurate beyond a strain of approximately $\varepsilon_3 = 2\times\varepsilon_{c1}$. Modeling of the concrete post-peak behavior in triaxial compression thus constitutes a limitation of the model in case of significant confinement. The following example helps to give a further insight into this limitation.

The test by Poinard, et al. (2010) is interested in the behavior of concrete at very high confinement level. It was conducted on a concrete cylinder of 40 N/mm² uniaxial compressive strength subjected to 200 N/mm² confinement, see Fig. 11. The sample was then subjected to increasing axial deviatoric stress. The computed response agrees with the experimental results in the first part of the test, until reaching a deviatoric stress of approximately 115 N/mm² and an axial strain equal to $2\times\varepsilon_{c1}$. However, the computed response beyond this level of stress completely differs from the experimental response, because the computed response then presents a softening behavior whereas the experimental results clearly indicate a hardening behavior. Very interesting information can be obtained from Poinard's test owing to the fact

that several unloading-reloading sequences have been applied to the sample. Indeed, the analysis of the slope of the unloading branches indicates that no damage develops in concrete under such very high confinement level, as these unloading branches remain parallel to the initial stiffness of the material. On the contrary, the model assumes that damage starts to develop in the concrete as soon as plasticity develops, as these two phenomena have been linked in the model. Consequently, significant damage develops during the numerical simulation of the triaxial test; this is confirmed by the degradation of the elastic properties that can be observed on the computed curves in Fig. 11. The fact that damage develops in the model for concrete under high confinement contributes to explain why the model is not able to properly capture the post-peak behavior of concrete in these situations. In order to enhance the modeling in case of important triaxial compressive stress states, it would be necessary to govern the evolutions of plasticity and damage with distinct internal variables. Yet, it is noted that this high level of triaxial confinement is very unusual in buildings; it only concerns very specific applications such as the study of impact loading in the design of nuclear vessels.

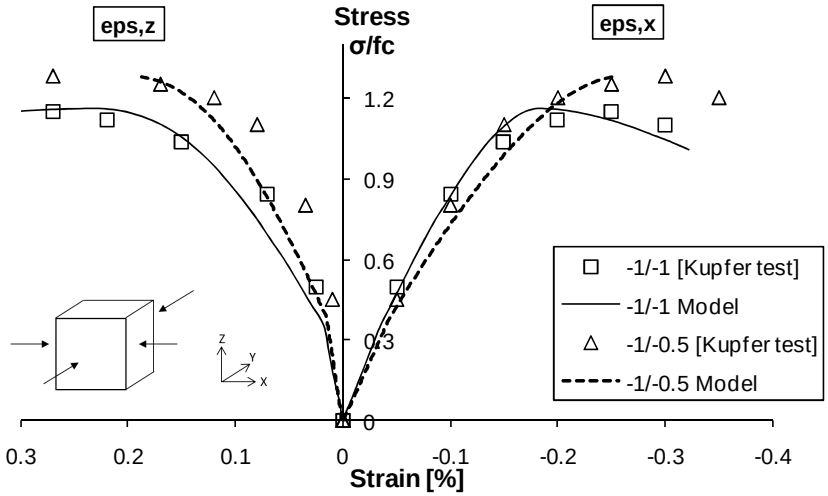

Fig. 9: Measured and computed results for concrete in biaxial compression test.

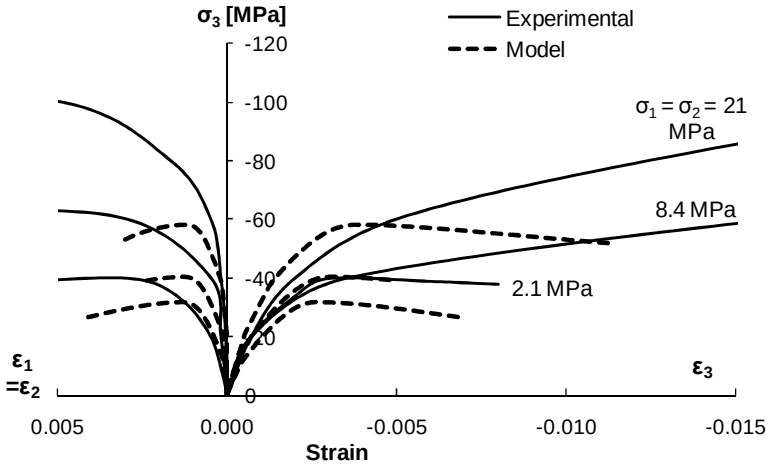

Fig. 10: Measured (Imran, 1994) and computed results for concrete in triaxial compression under three levels of confinement.

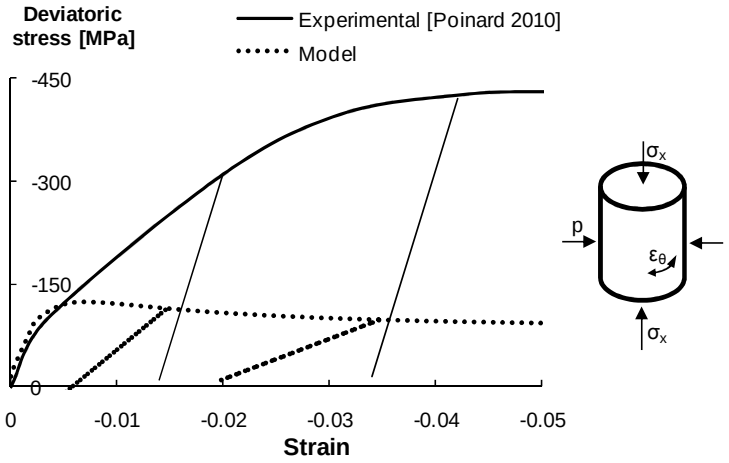

Fig. 11: Measured (Poinard, et al., 2010) and computed results for concrete in triaxial compression at 200 N/mm² confinement.

5.2. At high temperature

It is experimentally observed that the total strain that develops in heated concrete strongly depends on the applied stress during heating; therefore, transient tests aim to measure the total strain-temperature relationship for different load levels. The transient tests conducted by Anderberg and Thelandersson (1976) have been simulated using the new concrete model. In these tests, calcareous concrete samples have been subjected to constant applied stress and increasing temperature. Three levels of applied stress α were considered, with α defined as the ratio between the applied stress and the compressive strength at ambient temperature.

The measured and computed results given in Fig. 12 reasonably agree. The temperature at which the failure arises is well predicted by the model, as well as the decrease in total strain with increasing applied stress level during heating. The development of transient creep strain is thus accurately taken into account by the model.

The computed results show rather abrupt changes in the slope of the curves at every 100°C. This is due to the fact that the temperature-dependent laws of some parameters of the concrete model are defined as linear interpolations between discrete values defined every 100°C. This is the case, for instance, for the compressive strength the temperature-dependent law of which has been adopted from Eurocode. As a result, this abrupt variation in the derivative of the temperature-dependent laws is reflected on the results of Fig. 12. This effect is usually not perceived in numerical simulations of concrete elements because the model usually comprises an important number of integration points which reach the transition temperatures at different times.

Biaxial compression tests at high temperature have been conducted by Ehm and Schneider (1985). The experiments on siliceous concrete samples have been simulated and the comparison between measured and computed results is plotted in Fig. 13. In these steady-state tests, the samples are first heated and then subjected to stress increase in directions 1 and 2 simultaneously and of the same magnitude, whereas direction 3 is free.

The concrete model qualitatively captures the decrease in stiffness and equibiaxial compressive strength with temperature. Besides, the model takes into account the experimentally observed increase in the confinement effect with increasing temperature;

namely, the decrease in equibiaxial compressive strength is less pronounced than the decrease in uniaxial compressive strength at a given temperature.

It can be noted that the maximum relative stress $\sigma / f_{c,20}$ yield by the numerical simulations does not fit perfectly with the experimental results at high temperatures. This is due to the fact that the concrete tested by Ehm and Schneider does not follow the Eurocode model for the decrease in the uniaxial compressive strength, whereas the equibiaxial compressive strength at high temperature calculated in the model using Eq. (26) is related to the uniaxial compressive strength at high temperature prescribed by the Eurocode.

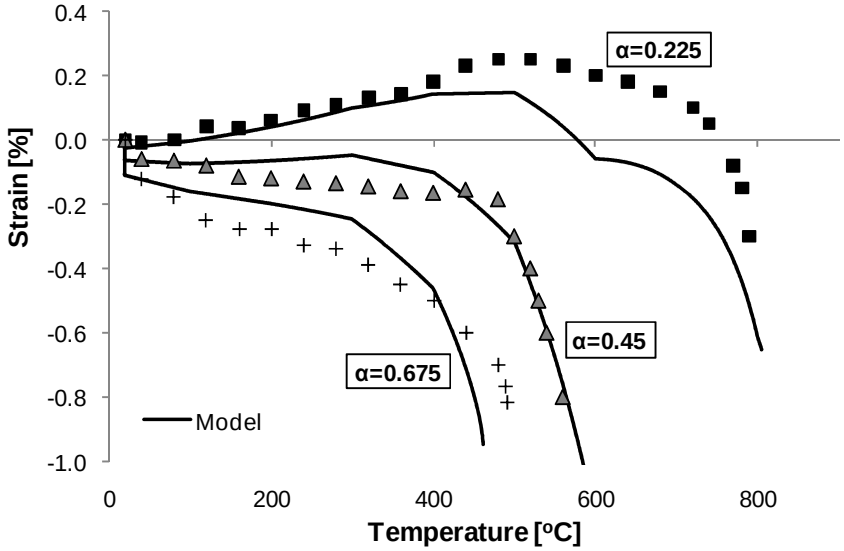

Fig. 12: Measured (Anderberg and Thelandersson, 1976) and computed results for concrete in transient tests for different applied stress levels.

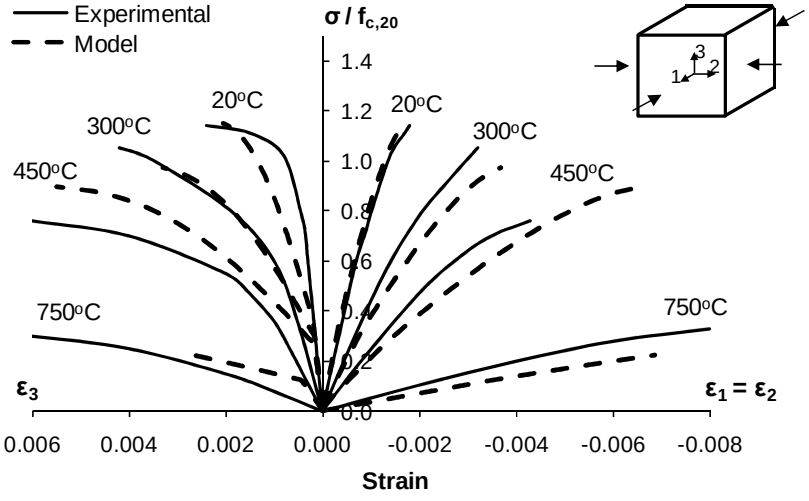

Fig. 13: Measured (Ehm and Schneider, 1985) and computed results for concrete in equibiaxial compressive loading at elevated temperatures.

6 Conclusion

This paper has presented a multiaxial constitutive model for concrete based on a plastic-damage formulation and taking into account the effect of high temperatures on the mechanical behavior. Combination of the elastoplastic and the damage theories offers an interesting framework for the development of a phenomenological model for concrete as it encompasses the capabilities of the plasticity theory for capturing the phenomena of dilatancy and permanent strains and the capabilities of damage theory for modeling of stiffness degradation and unilateral effect. Meanwhile, this approach is appealing with regard to the applicability to practical situations of structural fire engineering because it belongs to the class of continuum constitutive models based on a smeared crack approach. The proposed model adopted the fourth-order tensor representation of isotropic damage developed by Wu, et al. (2006) at ambient temperature, and extended its application to high temperatures.

The generalization of the multiaxial concrete model to take into account the effect of high temperatures is done by incorporating into the model the free thermal strain, the transient creep strain and proper relationships for the temperature-dependency of the material parameters. The original model of transient creep strain implemented in the model captures accurately this phenomenon including in performance-based situations, which may include cooling phases or load redistributions. The obtained multiaxial concrete model can therefore be used in any situation of unsteady temperature and multiaxial stress state; yet, it has been developed to yield back the same results as the uniaxial Eurocode concrete model in case of simple prescriptive uniaxial situations, which was found interesting as the Eurocode model has been widely used in the last decades and is well accepted by authorities and regulators for building design.

The concrete model has been implemented in the finite elements software SAFIR dedicated to the analysis of structures in fire. As it is a fully three-dimensional model it can be used for any stress state; besides, the particularization to plane stress states has been treated in order to provide a model for shell finite elements. In this paper, the model has been tested against experimental data at the material level in order to validate its ability to capture the different phenomena that develop in concrete at ambient and at high temperature. The concrete behavior is accurately captured in a large range of temperature and stress states using a limited number of parameters. Yet, the validity domain of the model does not include high levels of triaxial confinement because of the coupling assumption between damage and plasticity; in case of specific applications with high confinement such as the study of impact loading in the design of nuclear vessels, the constitutive model should use distinct internal variables to drive the evolution of plasticity and damage in the material.

The model has been developed for applications in structural fire engineering. In a forthcoming paper, several examples of numerical simulations of structural experiments will be presented, including a large-scale fire test.

REFERENCES

Abu Al-Rub, R.K. and Voyiadjis, G.Z., 2009. Gradient-enhanced Coupled Plasticity-anisotropic Damage Model for Concrete Fracture: Computational Aspects and Applications. *International Journal of Damage Mechanics*, 18(2), pp. 115-154.

Abu Al-Rub, R.K. and Kim, S.M., 2010. Computational applications of a coupled plasticity-damage constitutive model for simulating plain concrete fracture. *Engrg Fracture Mechanics*, 77(10), pp. 1577-1603.

Anderberg, Y. and Thelandersson, S., 1976. *Stress and deformation characteristics of concrete at high temperatures: 2 experimental investigation and material behavior model*. Bulletin 54, Lund Institute of Technology, Sweden.

Annerel, E., 2010. *Assessment of the residual strength of concrete structures after fire exposure*. Ph. D. Universiteit Gent.

ASTME - American Society for Testing and Materials, 2007. *ASTME119-00 - Standard Methods of Fire Test of Building Construction and Materials*. West Conshohocken, PA, USA.

Baker, G. and de Borst, R., 2005. An anisotropic thermomechanical damage model for concrete at transient elevated temperatures. *Phil. Trans. R. Soc. A.*, 363, pp. 2603-2628.

Carol, I., Rizzi, E. and Willam, K., 2001a. On the formulation of anisotropic elastic degradation. I. Theory based on a pseudo-logarithmic damage tensor rate. *International Journal of Solids and Structures*, 38, pp. 491-518.

Carol, I., Rizzi, E. and Willam, K., 2001b. On the formulation of anisotropic elastic degradation. II. Generalized pseudo-Rankine model for tensile damage. *International Journal of Solids and Structures*, 38, pp. 519-546.

CAST3M, 2003. *Commissariat à l'Energie Atomique*. Available at http://www-cast3m.cea.fr/.

CEB-FIB - Comité Euro-International du Béton-Fédération internationale du béton, 1990. *CEB-FIB Model code 1990 Bulletin d'information*. Lausanne, Switzerland.

Cervenka, J. and Papanikolaou, V.K., 2008. Three dimensional combined fracture-plastic material model for concrete. *International Journal of Plasticity*, 24, pp. 2192-2220.

Charras, T., 2010. Personnal communication, CEA, France.

Cicekli, U., Voyiadjis, G.Z. and Abu Al-Rub, R.K., 2007. A plasticity and anisotropic damage model for plain concrete. *International Journal of Plasticity*, 23, pp. 1874-1900.

de Borst, R. and Peeters, P., 1989. Analysis of concrete structures under thermal loading. *Computer methods in applied mechanics and engineering*, 77, pp. 293-310.

de Sa, C. and Benboudjema, F., 2011. Modeling of concrete nonlinear mechanical behavior at high temperatures with different damage-based approaches. *Materials and Structures*, 44, pp. 1411–1429.

Desmorat, R., Gatuingt, F. and Ragueneau, F., 2007. Nonlocal anisotropic damage model and related computational aspects for quasi-brittle materials. *Engineering Fracture Mechanics*, 74, pp. 1539–1560.

Dimia, M.S., Guenfoud, M., Gernay, T. and Franssen, J.M., 2011. Collapse of concrete columns during and after the cooling phase of a fire. *Journal of Fire Protection Engineering*, 21(4), pp. 245–263.

Ehm, C. and Schneider, U., 1985. The high temperature behavior of concrete under biaxial conditions. *Cement Concrete Res*, 15, pp. 27-34.

European Committee for Standardization, 1995. *CEN Eurocode 2 - Design of concrete structures - Part 1-2: General rules - Structural fire design. European Prestandard*. Brussels.

European Committee for Standardization, 2004-a. *CEN Eurocode 2 - Design of concrete structures - Part 1-2: General rules – Structural fire design.* Brussels.

European Committee for Standardization, 2004-b. *CEN Eurocode 4 - Design of composite steel and concrete structures - Part 1-2: General rules – Structural fire design.* Brussels.

Feenstra, P.H. and de Borst, R., 1996. A composite plasticity model for concrete. *International Journal of Solids and Structures*, 33, pp. 707-730.

Franssen, J.-M., 1993. *Thermal elongation of concrete during heating up to 700°C and cooling; Stress-strain relationship of Tempcore steel after heating up to 650°C and cooling*. Liege, Belgium : Univ. of Liege.

Franssen, J.-M., 2005. SAFIR: A thermal/structural program for modeling structures under fire. *Engineering Journal - A.I.S.C*, 42(3), pp. 143-158.

Gawin, D., Pesavento, F. and Schrefler, B.A., 2004. Modelling of deformations of high strength concrete at elevated temperatures. *Materials and Structures: Concrete Science and Engineering*, 37, pp. 218-236.

Gernay, T. and Franssen, J.-M., 2010. Consideration of transient creep in the Eurocode constitutive model for concrete in the fire situation. In*: Proceedings of the 6th International Conference on Structures in Fire, SiF'10, East Lansing, MI, 2010*, pp. 784-791.

Gernay, T. and Dimia, M.S., 2011. Structural behavior of concrete columns under natural fires including cooling down phase. In: Barros, H., Faria, R., Pina, C. and Ferreira, C. *Proceedings of The International Conference on Recent Advances in Nonlinear Models - Structural Concrete Applications*, Coimbra, Portugal 24-25 Nov. 2011. RAGRAF, pp. 637-656.

Gernay, T. and Franssen, J.-M., 2012. A formulation of the Eurocode 2 concrete model at elevated temperature that includes an explicit term for transient creep. *Fire safety journal*, 51, pp. 1-9.

Gernay, T., 2012-a. Effect of Transient Creep Strain Model on the Behavior of Concrete Columns Subjected to Heating and Cooling. *Fire Technology*. 48(2), pp. 313-329.

Gernay, T., 2012-b. *A constitutive model for concrete in the fire situation including transient creep and cooling down phases*. Ph. D. University of Liege, pp. 269.

Gopalaratnam, V.S. and Shah, S. P., 1985. Softening Response of Plain Concrete in Direct Tension. *ACI Journal Proceedings*, 82(3), pp. 310-323.

Grassl, P., Lundgren, K. and Gylltoft, K., 2002. Concrete in compression: a plasticity theory with a novel hardening law. *International Journal of Solids and Structures*, 39, pp. 5205-5223.

Grassl, P. and Jirasek, M., 2006. Damage-plastic model for concrete failure. *International Journal of Solids and Structures*, 43, pp. 7166-7196.

Heinfling, G., 1998. *Contribution à la modélisation numérique du comportement du béton et des structures en béton armé sous sollicitations thermo-mécaniques à hautes températures*. Ph. D. thesis INSA Lyon.

Hillerborg, A., Modeer, M. and Petersson, P.E., 1976. Analysis of crack formation and crack growth in concrete by means of fracture mechanics and finite elements. *Cement and concrete research*, 6(6), pp. 773-782.

Imran, I., 1994. *Applications of nonassociated plasticity in modeling the mechanical response of concrete*. Ph. D. thesis University of Toronto.

ISO - International Standards Office, 1975. *ISO834 – Fire resistance tests - elements of building construction*. Geneva: ISO.

Ju, J., 1989. On energy-based coupled elasto-plastic damage theories: constitutive modeling and computational aspects. *Int. J. Solids Struct*., 25, pp. 803-833.

Ju, J., 1990. Isotropic and anisotropic damage variables in continuum damage mechanics. *J. Eng. Mech. ASCE*, 116(12), pp. 2764–2770.

Karsan, I.D. and Jirsa, J.O., 1969. Behavior of concrete under compressive loadings. *J. Struct. Div. ASCE*., 95(12), pp. 2535-2563.

Khennane, A. and Baker, G., 1992. Thermoplasticity Model for Concrete under Transient Temperature and Biaxial Stress. *Proc. R. Soc. Lond*., 439, pp. 59-80.

Kodur, V.K.R., 1999. Performance-based Fire Resistance Design of Concrete-filled Steel Columns. *J. Constr. Steel Res. Institute*, 51, pp. 21-36.

Koiter, W.T., 1953. Stress-strain relations, uniqueness and variational theorems for elastic-plastic materials with a singular yield surface. *Q. Appl. Math*., 11, pp. 350-354.

Krätzig, W. and Pölling, R., 2004. An elasto-plastic damage model for reinforced concrete with minimum number of material parameters. *Computers and Structures*, 82(15-16), pp. 1201-1215.

Kupfer, H.B., Hilsdorf, H.K. and Rüsch, H., 1969. Behavior of concrete under biaxial stresses. *Journal of the American Concrete Institute*, 66, pp. 656-666.

Kupfer, H.B. and Gerstle, K.H., 1973. Behavior of concrete under biaxial stresses. *Journal of the Engineering Mechanics Division ASCE*., 99, pp. 853-866.

Lee, J. and Fenves, G.L., 1998. Plastic-damage model for cyclic loading of concrete structures. *Journal of Engineering Mechanics ASCE*, 124(8), pp. 892-900.

Li, L. and Purkiss, J., 2005. Stress-strain constitutive equations of concrete material at elevated temperatures. *Fire Safety Journal*, 40, 669-686.

Li, T. and Crouch, R., 2010. A C2 plasticity model for structural concrete. *Computers and Structures*, 88(23-24), pp. 1322–1332.

Li, Y.H. and Franssen, J.M., 2011. Test results and model for the residual compressive strength of concrete after a fire. *J. of Struct. Fire Eng.*, 2(1), pp. 29-44.

Lubliner, J., Oliver, J., Oller, S. and Onate, E., 1989. A plastic-damage model for concrete. *Int. J. Solids Struct.*, 25(3), pp. 299-326.

Luccioni, B.M., Figueroa, M.I. and Danesi, R.F., 2003. Thermo-mechanic model for concrete exposed to elevated temperatures. *Engineering Structures*, 25(6), 729-742.

Maréchal, J.C., 1970. *Variations in the modulus of elasticity and poisson's ratio with temperature.* In: ACI. *Int. Seminar on CNR*. Berlin.

Matallah, M. and La Borderie, C., 2009. *Inelasticity-damage-based model for numerical modeling of concrete cracking*. *Engineering Fracture Mechanics*, 76, pp. 1087-1108.

Mazars, J., 1984. *Application de la mécanique de l'endommagement au comportement non linéaire et à la rupture du béton de structure*. Ph. D. thesis Université Paris VI.

Meacham, B.J. and Custer, R.P.L., 1992. Performance-based Fire Safety Engineering: An Introduction of Basic Concepts. *J. Constr. Steel Res. Institute*, 7, pp. 35–54.

Meschke, G., Lackner, R. and Mang, H., 1998. An anisotropic elastoplastic-damage model for plain concrete. *Int J for Numerical Methods in Engineering*, 42(4), pp. 703-727.

Nechnech, W., Meftah, F. and Reynouard, J.M., 2002. An elasto-plastic damage model for plain concrete subjected to high temperatures. *Engineering Structures*, 24, pp. 597-611.

Onate, E., Oller, S., Oliver, J. and Lubliner, J., 1993. A constitutive model for cracking of concrete based on the incremental theory of plasticity. *Engineering Computations: Int J for Computer-Aided Engineering*, 5(4), pp. 309-319.

Ortiz, M., 1985. A constitutive theory for the inelastic behavior of concrete. *Mechanics of Materials*, 4, pp. 67-93.

Poinard, C., Malecot, Y. and Daudeville, L., 2010. Damage of concrete in a very high stress state: experimental investigation. *Materials and Structures*, 43, pp. 15-29.

Pramono, E. and Willam, K.J., 1989. Implicit integration of composite yield surfaces with corners. *Engng Comput.*, 7, pp. 186-197.

Ramtani, S., 1990. *Contribution à la modélisation du comportement multiaxial du béton endommagé avec description du caractère unilatéral*. Ph. D. thesis Université de Paris VI E.N.S. de Cachan.

Richard, B., Ragueneau, F., Cremona, C. and Adelaide, L., 2010. Isotropic continuum damage mechanics for concrete under cyclic loading: Stiffness recovery, inelastic strains and frictional sliding. *Engineering Fracture Mechanics*, 77, pp. 1203–1223.

Rots, J.G., 1988. Computational modelling of concrete fracture. Ph. D. thesis, Delft University of Technology.

Saritas, A., and Filippou, F.C., 2009. Numerical integration of a class of 3d plastic-damage concrete models condensation of 3d stress-strain relations for use in beam finite elements. *Eng. Struct.*, 31(10), pp. 2327-2336.

Schneider, U., 1985. *Properties of materials at high temperatures: concrete*. Kassel, Germany: RILEM.

Schneider, U., 1988. Concrete at high temperatures - a general review. *Fire Safety Journal*, 13, pp. 55-68.

Simo, J.C. and Hughes, T.J.R., 1998. *Computational inelasticity*. New York: Springer.

Taqieddin, Z., Voyiadjis, G.Z., ASCE, F. and Almasri, A.H., 2012. Formulation and verification of a concrete model with strong coupling between isotropic damage and elastoplasticity and comparison to a weak coupling model. *Journal of Engineering Mechanics A.S.C.E.*, 138, pp. 530–541.

Thelandersson, S., 1987. Modelling of combined thermal and mechanical action in concrete. *ASCE J. Engrg. Mech*., 113, pp. 893-906.

Vonk, R.A., 1992. Softening of concrete loaded in compression. Ph. D. thesis, Eindhoven University of Technology.

Voyiadjis, G.Z., Taqieddin, Z. and Kattan, P., 2008. Anisotropic damage-plasticity model for concrete. *Internation Journal of Plasticity*, 24(10), pp. 1946–1965.

Voyiadjis, G.Z., Taqieddin, Z. and Kattan, P., 2009. Theoretical formulation of a coupled elastic-plastic anisotropic damage model for concrete using the strain energy equivalence concept. *Internation Journal of Damage Mechanics*, 18(7), pp. 603–638.

Willam, K.J. and Warnke, E.P., 1974. Constitutive model for the triaxial behavior of concrete. *Seminar on Concrete Structures Subjected to Triaxial Stresses. Int. Assoc. of Bridge and Struct. Engng. Conf.*, Bergamo, Italy.

Wu, J.Y., Li, J. and Faria, R., 2006. An energy release rate-based plastic-damage model for concrete. *International Journal of Solids and Structures*, 43, pp. 583–612.